GCNA: GUARDIAN OF THE GENOME

APPROVED BY SUPERVISORY COMMITTEE

Michael Buszczak, Ph.D.

John Abrams, Ph.D.

Rolf Brekken, Ph.D.

Eric Olson, Ph.D.

DEDICATION

I would like to dedicate this to my mother, Lynne, to my father, Jay, to my sister, Jaime, to my boyfriend, Coy, and to my dogs, Scully and Mulder.

GCNA: GUARDIAN OF THE GENOME

by

COURTNEY DAVEE GOLDSTEIN

DISSERTATION

Presented to the Faculty of the Graduate School of Biomedical Sciences

The University of Texas Southwestern Medical Center at Dallas

In Partial Fulfillment of the Requirements

For the Degree of

DOCTOR OF PHILOSOPHY

The University of Texas Southwestern Medical Center at Dallas

Dallas, Texas

May, 2020

ACKNOWLEDGEMENTS

I would like to thank my mentor, Michael Buszczak, first and foremost. Without his support and advice throughout my graduate career, I would not have reached this point. I would also like to thank all the former and current members of the Buszczak lab that I overlapped with for their friendship and advice. I would like to give a special thanks to Varsha, who started the screen and GCNA project with me. I would like to thank my thesis committee, Drs. John Abrams, Rolf Brekken, and Eric Olson, for their advice and experimental suggestions throughout my graduate career. Also, I would like to thank the NA8 floor for being a constant source of inspiration for experiments as well as laughter and the GEMS community for their invaluable input and generosity in sharing reagents.

I am extremely grateful to all my friends that I have gained during my graduate career both from UTSW and elsewhere. Graduate school is an emotional rollercoaster, and my friends have helped me keep my sanity during this wild ride. I am also very grateful for Coy Goodson. He has been my rock, and he smooths out the difficult times. I am incredibly grateful for his editorial skills throughout my graduate career. Our two wonderful and mischievous dogs are a constant source of joy and entertainment. Lastly, I would like to thank my family for their unconditional love and support. My parents have always fostered my intellectual curiosity and without them I would not have made it to where I am today.

GCNA: GUARDIAN OF THE GENOME

Publication No. 3

Courtney DaVee Goldstein

The University of Texas Southwestern Medical Center at Dallas, Graduation Year

Supervising Professor: Michael Buszczak, Ph.D.

The propagation of species depends on the ability of germ cells to protect their genome in the face of numerous exogenous and endogenous threats. While germ cells employ a number of know repair pathways, specialized mechanisms that ensure high-fidelity replication, chromosome segregation, and repair of germ cell genomes remain incompletely understood. Here, we identify Germ cell nuclear acidic peptidase (GCNA) as a conserved regulator of genome stability in flies, worms, zebrafish and human germ cell tumors. GCNA contains an acidic intrinsically disordered region (IDR) and a protease-like SprT domain. In addition to chromosomal instability and replication stress, *Gcna* mutants accumulate DNA-protein crosslinks (DPCs). GCNA acts in parallel with a second SprT domain protein Spartan.

Structural analysis reveals that while the SprT domain is needed to limit meiotic and replicative damage, much of GCNA's function maps to its IDR. This work shows GCNA protects germ cells from various sources of damage, providing novel insights into conserved mechanisms that promote genome integrity across generations.

TABLE OF CONTENTS

PRIOR PUBLICATIONS

Bhargava V[*], Goldstein CD[*], Russell L[*], Xu L*, Ahmed M, Li W, Casey A, Servage K, Kollipara R, Picciarelli Z, Kittler R, Yatsenko A, Carmell M, Orth K, Amatruda JF[,+], Yanowitz JL[+], Buszczak M[+] "GCNA preserves genome integrity and fertility across species." (Accepted at Developmental Cell)

Aguilera KY, Rivera LB, Hur H, Carbon JG, Toombs JE, Goldstein CD, Dellinger MT, Castrillon DH, and Brekken RA. "Collagen signaling enhances tumor spread after anti-VEGF therapy in a murine model of PDAC." Cancer Res. 2014. 74(4):1032-1044. PMC3944405

LIST OF FIGURES

CHAPTER ONE

CHAPTER THREE

CHAPTER FOUR

LIST OF APPENDICES

LIST OF DEFINITIONS

Asl – Asterless

ATM – Ataxia-Telangiectasia Mutated

ATR– Ataxia-Telangiectasia and RAD3 related

Cnn – Centrosomin

Chk1 – Checkpoint Kinase 1

CO – Crossover

DPC – DNA-Protein Crosslink

DSB – Double-Strand Breaks

dsDNA – double-strand DNA

GCNA – Germ Cell Nuclear Acidic Peptidase

GCT – Germline Cell Tumor

GSC – Germline Stem Cell

HR – Homologous Recombination

HU – Hydroxyurea

γH2Av – γ Histone 2A variant

IDR – Intrinsically Disordered Region

ipMT – Interpolar Microtubules

K-fibers – Kinetochore Fibers

MSI – Microsatellite Repeat Instability

RADAR – Rapid Approach to DNA Adduct Recovery

RPA – Replication Protein A

ssDNA – single-strand DNA

γTuRC – γ Tubulin Ring Complex

WT – Wildtype

ZnF – Zinc Finger

CHAPTER ONE
Introduction

Germ cells

Germ cells transfer genetic information from parents to their progeny, and any change in germline DNA is inherited by succeeding generations. Therefore, germ cell DNA must be protected from potentially deleterious internal and external assaults. An advantage of sexual reproduction stems from the ability to generate variation by exchange of chromosomal segments during meiosis. Hundreds of DNA double-strand breaks (DSBs) are initiated simultaneously during meiosis, which if generated in most other cell types would induce cell death or introduce chromosomal aberrations. Germ cells, however, execute the formation and repair of these breaks while preventing their deleterious effects from becoming pervasive throughout the genome. Germ cells also extensively reprogram their epigenome to a state that fosters totipotency (Kurimoto and Saitou, 2018; Tang et al., 2016). A byproduct of epigenetic reprogramming is reactive aldehydes (Walport et al., 2012). These reactive aldehydes can crosslink proteins to DNA which can interfere with most chromatin biology. Yet despite these challenges that germs cells face, germ cells have a 10 to 20-fold lower mutational burden than somatic cells (Milholland et al., 2017). The mechanisms underlying the robustness of germ cells in the face of extensive DNA damage, however, remain poorly understood. Thus, enhancing our understating of germ cell biology will provide useful insights into regeneration, genome surveillance, and adults stem cell systems.

Drosophila as a model organism to study the germline

The *Drosophila* female germline is an excellent model to study germ cell biology because it is a well-defined and easily manipulated system. The *Drosophila* ovary is made up of 15-20 repeating units called ovarioles (Figure 1.1). At the anterior of each ovariole resides a structure referred to as the germarium which houses two to three germline stem cells (GSCs) and developing cysts. The GSCs divide asymmetrically, producing one daughter cell that will continue to self-renew and one differentiating daughter cell referred to as the cystoblast (CB). The CB will go through four synchronous rounds of division with incomplete cytokinesis to create a 16-cell cyst. Of these 16 cells, one will become the oocyte and the others will become nurse cells which support the developing oocyte.

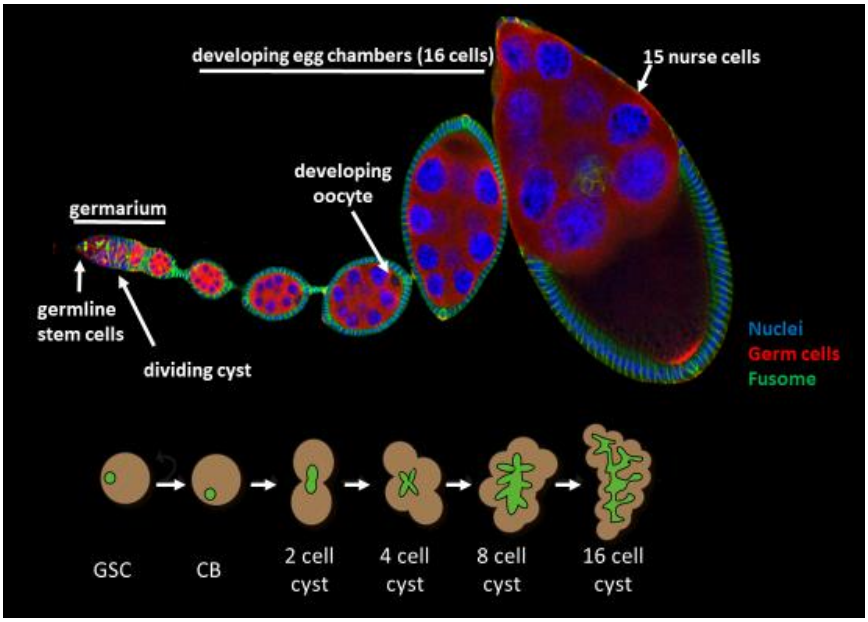

Figure 1.1. The *Drosophila* ovariole. Germline stem cells (GSCs) reside at the anterior tip of the germarium marked by a founded fusome (1B1:green). Germ cells are marked with Vasa (red). The cystoblast (CB) is the differentiating daughter cell and goes through four synchronous rounds of division. Of the resulting 16 cells, one will become the oocyte and the other 15 will become nurse cells. DNA is stained with DAPI.

Meiosis: the essence of heredity

Meiosis is the process that forms a haploid gamete from a diploid cell; thus, a cell goes through one round of replication followed by two rounds of cell division. Without meiosis, the progeny of sexually reproducing species would double their genomic content with each successive generation. During prophase I of meiosis, DSB are induced to initiate meiotic recombination. Recombination creates physical links that aid in holding homologous chromosomes together until the homologs need to be separated. Another benefit of meiotic

recombination is that it breaks up the combination of alleles on a single chromosome to facilitate adaptive evolution.

In *Drosophila,* the oocytes within the 16-cell cyst experience programmed DSBs during meiosis (Figure 1.2). Meiotic DSBs are induced by Spo11, an evolutionarily conserved topoisomerase-like protein which forms a covalent DNA-protein intermediate (Keeney et al., 1997). Spo11 is endonucleolytically released by the MRN complex consisting of Mre11, Rad50, and Nbs1, resulting in a free Spo11 bound to a short oligo (Neale et al., 2005). Further nucleolytic processing reveals a 3' overhang is subsequently coated by Rad51. Rad51 coated filaments initiate strand invasion which leads to homologous recombination (Sung, 1994). Two kinases, Ataxia-telangiectasia mutated (ATM) and ataxia-telangiectasia and RAD3 related (ATR), are needed for efficient signal transduction in response to a DSB. One of the protein targets for these kinases is the histone 2A variant H2Av in *Drosophila* or H2AX in mammals (Joyce et al., 2011). Phosphorylated H2AX amplifies the DSB signal and can spread across megabases. Consequently, γH2Av or γH2AX is the first step of a DSB repair process that can be visualized histologically.

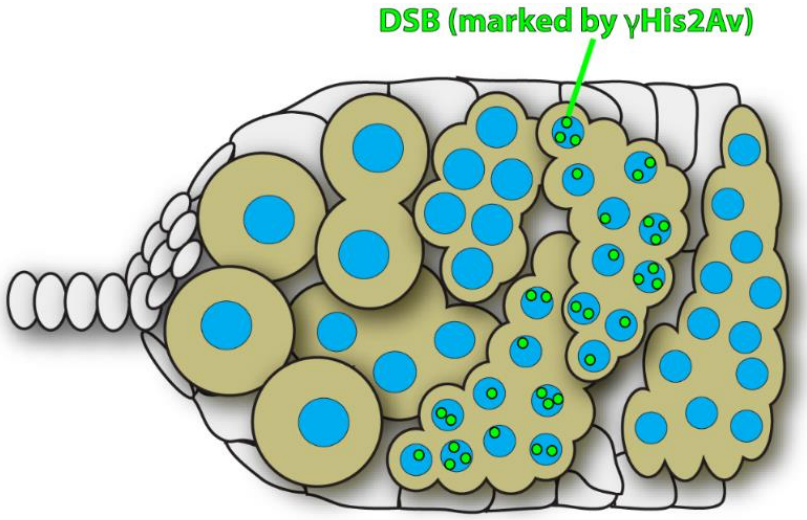

Figure 1.2. Meiosis in the *Drosophila* germarium. The 16-cell cyst undergoes programed DSBs during meiosis which can be visualized as γH2Av foci (green). The breaks are repaired before the cysts bud off from the germarium. Germ cells are tan and somatic cells are white.

DNA-protein crosslinks

DNA-protein crosslinks (DPCs) form when a protein becomes covalently crosslinked to DNA. DPCs represent particularly toxic lesions because they interfere with most chromatin-based processes including DNA replication, transcription, and chromatin remodeling (Stingele et al., 2017; Vaz et al., 2017). A DPC is a large, bulky adduct that can present a major challenge to repair because any protein that has access to DNA has the potential to become crosslinked. This large variety in adducts poses a challenge for both sensing and repairing the lesion. Failure to repair a DPC will lead to replication fork stalling and ultimately fork collapse, creating DSBs and genomic instability (Stingele et al., 2017; Vaz et al., 2017). Three major

pathways are known to resolve DPCs: protease-dependent repair, nuclease-dependent repair, and direct crosslink hydrolysis. For the context of this chapter only protease-dependent repair will be discussed.

DPC formation

DPCs can be categorized into three different groups based on how they form. First, non-enzymatic proteins can become nonspecifically crosslinked to DNA due to the presence of a crosslinker. Several reactions important for epigenetic reprograming of germ cells, such as histone demethylation, produce reactive aldehydes (Walport et al., 2012). These reactive aldehydes have the potential to crosslink any protein within the vicinity of DNA. Crosslinkers can also be introduced exogenously; for example, many chemotherapeutics are crosslinkers, including cisplatin and melphalan (Chvalova et al., 2007). Second, enzymatic proteins can form a temporary and typically short-lived DPC during their normal catalytic function, including topoisomerases, DNA methyltransferases, and DNA polymerases. These normally short-lived intermediates can become stabilized in the presence of an enzyme poison or a shift in the topography of the chromatin (Pommier et al., 2014). Third, a DPC-like trapping can occur when a protein becomes so stably bound to DNA that it acts like a DPC, and the cell experiences DPC-like consequences even though the protein is not covalently crosslinked to DNA. For example, PARP1 inhibitors, such as olaparib, rucaparib, and niraparib, cause PARP1 DPC-like trapping (Murai et al., 2012).

DPC clearance by proteolysis

Recent work has shown that the Wss1/Spartan proteins play an important role in clearing DPCs. When a replication fork stalls due to the presence of a DPC, Spartan is recruited to clear the DPC (Lopez-Mosqueda et al., 2016; Stingele et al., 2016; Vaz et al., 2016). Spartan's activity is tightly regulated. Spartan is only fully active in the presence of single-strand DNA (ssDNA) which allows for processing of the DPC(Stingele et al., 2016). Conversely, Spartan will inactivate itself with a self-cleavage event in the presence of dsDNA. This "off-switch" is thought to protect undamaged chromatin from Spartan's activity. Once fully active, Spartan will chew up the adduct into a much smaller lesion that a translesion synthesis (TLS) polymerase can bypass. Spartan's metalloprotease domain, the SprT domain, is rather promiscuous, so it can accommodate a variety of proteins and types of crosslinks. Spartan's activity has been shown to be tightly linked to replication as it is a constitutive component of the replication machinery (Larsen et al., 2019; Stingele et al., 2016; Vaz et al., 2016). Spartan also contributes to genome stability during replication by releasing activated Chk1 from chromatin so it can stabilize replication forks (Halder et al., 2019).

Causes and consequences of replication stress

Faithful replication of the genome is critical not only to ensure that an accurate copy of the genome is inherited in each daughter cell but also that the chromosomes are segregated properly. Replication stress is a major cause of genome instability because errors that occur during replication can lead to missegregation of chromosomes (Halazonetis et al., 2008; Magdalou et al., 2014). Three major sources of replication stress are discussed below: physical

blocks, inappropriate replication origin firing, and interference between replication and transcription.

Causes of replication stress

Physical blocks on DNA, such as DPCs, abasic sites or DNA secondary structure, are a source of replication stress. Physical blocks cause replication fork stalling and can eventually lead to their collapse. TLS polymerases and post-replication repair pathways are needed to bypass many of these lesions (Sale et al., 2012).

Inappropriate firing of replication origins is another source of replication stress. Excessive firing of replication origins leads to depletion of limiting resources during replication. If dNTP pools are depleted due to excessive firing, for example this can lead to replication stress and decrease cell viability (Mantiero et al., 2011). Also, Replication Protein A (RPA) can become limited with excessive origin firing (Toledo et al., 2013). RPA coats ssDNA to protect it, and lack of RPA coating ssDNA results in unprotected ssDNA. Uncoated ssDNA is vulnerable to nuclease attack, and forks with a buildup of uncoated ssDNA are more prone to breakage (Toledo et al., 2013). On the other hand, a deficiency of origin firing can lead to unreplicated DNA when the cell enters mitosis (Mankouri et al., 2013). Unreplicated loci on a chromosome results in anaphase bridges. These bridges can lead to chromosome breaks which usually cause unequal segregation of genetic material.

Lastly, interference from transcription machinery is a source of replication stress. Transcription machinery and replication machinery share the same template and thus are prone to collisions. Further, transcription and replication converging causes supercoiling which is

another source of replication stress (Bermejo et al., 2009; Tuduri et al., 2009). Extremely large genes are at a higher risk for convergence of transcription and replication machineries because they are transcribed throughout the cell cycle (Helmrich et al., 2011). These genes often overlap with common fragile sites on chromosomes.

Consequences of replication stress

Chronic replication stress can lead to erroneous centrosome replication (Wilhelm et al., 2014); however, the mechanism that causes additional centrosome amplification is unclear. These extra centrosomes promote multipolar mitosis which often leads to unequal chromosome segregation (Wilhelm et al., 2014). Multipolar mitosis favors improper attachment of microtubules to the kinetochores, resulting in lagging genetic material.

Replication stress can also lead to mitotic errors. Unreplicated loci form anaphase bridges (Mankouri et al., 2013). These bridges are prone to break, and the chromosomal fragments can segregate unequally. Further, the chromosomal fragments can form a micronucleus, which is a tiny nucleus of lagging or fragmented chromosomes that does not become incorporated into the main nucleus. A micronucleus can be viewed as a footprint of mitotic error because it can be seen in interphase cells. Micronuclei have defective cytoplasmic-nuclear trafficking, so they do not maintain proper communication with the cell including propagation of DNA damage response signaling (Crasta et al., 2012). Micronuclei have an abnormal nuclear envelope which are susceptible to bursting (Hatch et al., 2013). When the nuclear envelope bursts, the DNA inside is subject to cytoplasmic nucleases which can cause DSB. Due to the improper signaling in the DNA damage response in micronuclei,

a cell with DNA damage can enter mitosis and the chromosomal fragments can be religated randomly into the genome. This process is thought to lead to chromothripsis over multiple cell cycles, in which a chromosome shatters and religates randomly (Ly et al., 2017).

Cellular response to replication stress

A hallmark of replication stress is the accumulation of ssDNA at replication forks. RPA forms filaments around ssDNA to protect it. These RPA filaments also act as a scaffold for stress response machinery including the master replication stress kinase ATR. ATR has two core functions in responding to replication stress: (1) local function—stabilizing stalled replication forks and (2) global function—cell cycle arrest and repression of late replication origins. While the mechanism is not completely understood, ATR phosphorylates many components of the replisome and this is thought to keep the fork in a replication competent state (Cortez et al., 2004; Couch et al., 2013; Lopes et al., 2001; Tercero and Diffley, 2001). ATR also suppresses late firing replication origins when dNTP pools become limiting (Zegerman and Diffley, 2010). In addition, ATR phosphorylates Chk1 kinase, which amplifies the stress response signal and delays the onset of mitosis (Koundrioukoff et al., 2013). Thus, ATR contributes to limiting genome instability during DNA replication.

Gynandromorphs

Gynandromorphs are when an organism is half male and half female. In *Drosophila,* four previously isolated alleles give rise to gynandromorphs at an elevated rate: *ncd*, *Horka*^{D},

mit, and *pal*. Of these four, only *ncd* and *Horka*^{D} have been mapped to a gene. The *ncd* gene encodes a minus end directed motor in the kinesin-14 family (Hatsumi and Endow, 1992). It is required for spindle assembly in oocytes and spindle attachment to chromosomes in the embryo (Endow and Komma, 1996; Sköld et al., 2005). The maternal X chromosome is almost exclusively lost in embryos in the first division from mothers homozygous for *ncd* (Nelson and Szauter, 1992). *Horka*^{D} acts as an antimorphic allele of lodestar (lds) in which the A777T mutation results in the mutant protein having a higher affinity for chromatin (Szalontai et al., 2009). *Horka*^{D} destabilizes the paternal chromosomes in the sperm leading to a higher frequency of these chromosomes being lost in the embryo. The loss of the paternal unstable chromosomes leads diplo/halpo mosaics (XX/XO) or gynandromorphs. Now *Gcna*^{KO} is a fifth allele that produces gynandromorphs at an elevated rate. Gynandromorphs are produced from *Gcna*^{KO} because of the loss of an X chromosome due to mitotic errors.

CHAPTER TWO
Materials and Methods

DROSOPHILA

Immunofluorescence

Adult ovaries were stained according to (Tastan et al., 2010). Ovaries were dissected in 1x PBS. Tissue was fixed for 10 minutes with gentle rocking in 4% formaldehyde (EM grade) in PBS. After fixation, ovaries were washed four times in PBT (PBS + 0.5% BSA + 0.3% Triton-X 100) at RT for 10 minutes. Primary antibodies were incubated overnight at 4°C. Ovaries were then washed four times with PBT for 10 minutes, incubated for five hours with secondary antibodies. Ovaries were then washed and mounted in VectaShield Mounting medium with DAPI (Vector Laboratories).

Drosophila embryos were stained according to (Mani et al., 2014). Embryos were collected, dechorionated in 50% bleach, and fixed in 50% heptane, 50% fixative (3 parts fixing buffer, 1.33X PBS and 67mM EGTA :1 part 37% formaldehyde) for 10 mins. Embryos were then washed and devitellinized in methanol (MeOH) and stored at -20°C. Before staining, embryos were washed in a rehydration series consisting of 70%MeOH: 30%PBST, 50%MeOH: 50%PBST, 30%MeOH:70% PBST and finally 100% PBST for 5 minutes each, where PBST is PBS with 0.2% Triton X. Embryos were blocked in 10% normal goat serum for 1 hour.

The following primary antibodies were used: mouse anti gamma-H2AV (DSHB unc93.5.3.1) (30:200), rabbit anti-gamma-H2Av (Kim McKim) (1:500), rabbit anti-C(3)G (Mary Lilly) (1:3000) (Hong et al., 2003), rabbit anti-RPA (1:500) (Terry Orr-Weaver from

Fisher and Cotterill labs), rabbit anti-Top2 (T. Hsieh and D. Ardnt-Jovin) (1:400), mouse anti-Hts (1B1) (DSHB) (1:20), rat anti-Vasa (DSHB) (1:20), rabbit anti-GFP (1:1,000) (Life Technologies), rat anti-HA 3F10 (Roche), and fluorescence-conjugated secondary antibodies (Jackson Laboratories)(1:300).

Western blot analysis

Proteins extracts were separated by SDS-PAGE and transferred onto a nitrocellulose membrane. The following primary antibodies were used: rabbit anti-Top2 (T. Hsieh and D. Ardnt-Jovin) (1:2000), rat anti-Vasa (DSHB) (1:200), mouse anti-actin (DSHB) (1:100), rat anti-HA 3F10 (Roche) (1:2000). The secondary antibodies were anti-mouse IgG HRP (Jackson Laboratories) (1:2000), anti-rabbit IgG HRP (Jackson Laboratories) (1:2000), and anti-rat IgG HRP (Jackson Laboratories) (1:2000).

DNA-protein crosslink isolation

DPCs were isolated and detected using a modified rapid approach to DNA adduct recovery (RADAR) assay wherein the tissue was lysed in 10 mM Tris-HCl pH 6.8, 6 M GTC, 1% dithiothreitol, 20 mM EDTA, 4% Triton X, 1% sarkosyl (Kiianitsa and Maizels, 2013; Vaz et al., 2016). The DNA was ethanol precipitated by adding an equal volume of 100% ethanol to the lysis buffer and incubated at -20°C for five minutes. The pellet was washed three times in wash buffer (20 mM Tris-HCL pH 6.8, 150 mM NaCl and 50% ethanol). The nucleic acid pellet was solubilized in 8 mM NaOH. For *Drosophila*, the ovaries were dissected in cold Graces media and lysed for RADAR. Embryos were 0-2hrs old. Embryos were dechorionated

in 50% bleach for 2 minutes and then rinsed thoroughly with water before lysis. The zebrafish embryos were lysed at the 1000 cell stage. DNA concentration was measured using PicoGreen (Invitrogen) according to the manufacturer's instructions.

DNA and DNA-protein crosslink detection

DNA was detected by blotting the DNA with a slot blot vacuum manifold (Biorad) onto a positively charged nylon membrane. The membrane was probed with mouse anti-dsDNA (Abcam) (1:2000). Specific proteins were detected by normalizing to DNA concentration and digesting with benzonase. The proteins were separated on a polyacrylamide gel and silver stained (Sigma).

Immunoprecipitation

For overexpression in S2 cells, the Gcna construct was cloned into pAFHW (Drosophila Gateway Vector Collection). S2 cells were transfected with the expression constructs using Effectene (Qiagen). Cells were lysed (50mM Tris pH8.0, 137 mM NaCl, 1mM EDTA, 10mM NaF, 1% Triton X100, 10% glycerol, Roche protease inhibitor cocktail) and were applied to FLAG sepharose beads (Sigma) for 6.5 hours. The beads were washed three times in ice cold lysis buffer and the protein was eluted with 0.5 mg/mL 3x FLAG peptide (Sigma) overnight. The protein was applied to HA sepharose beads (Roche) for 8 hours. The beads were washed three times in ice cold lysis buffer, and bound proteins were retrieved by boiling the beads. Samples were run on SDS-PAGE gel and stained with Coomassie blue dye prior to analysis by mass spectrometry.

Mass spectrometry analysis

Protein gel bands were excised before being reduced with DTT and alkylated with iodoacetamide. Samples were digested overnight at 37°C using trypsin. Tryptic peptides were de-salted via solid phase extraction (SPE). LC-MS/MS experiments were performed on a Thermo Scientific EASY-nLC liquid chromatography system coupled to a Thermo Scientific Orbitrap Fusion Lumos mass spectrometer. To generate MS/MS spectra, MS1 spectra were first acquired in the Orbitrap mass analyzer (resolution 120,000). Peptide precursor ions were then isolated and fragmented using high-energy collision-induced dissociation (HCD). The resulting MS/MS fragmentation spectra were acquired in the ion trap. MS/MS spectral data was searched using Proteome Discoverer 2.1 software (Thermo Scientific) against entries included in the *Drosophila melanogaster* Uniprot protein database. Search parameters included setting Carbamidomethylation of cysteine residues (+57.021 Da) as a static modification and oxidation of methionine (+15.995 Da) and acetylation of peptide N-termini (+42.011 Da) as dynamic modifications. Precursor and product ion mass tolerances of 15 ppm and 0.6 Da were used, respectively. Peptide spectral matches were adjusted to a 1% false discovery rate (FDR) and additionally proteins were filtered to a 5% FDR. Proteins were quantified by area values determined via label-free quantitation using Proteome Discoverer 2.1 software. Complete protein lists from raw data are included as Tables S1-3.

Generating the *Gcna^{KO}* alleles

To generate the *Gcna^{KO}* allele, guide RNAs were designed using http://tools.flycrispr.molbio.wisc.edu/targetFinder and synthesized as 5'- unphosphorylated oligonucleotides (see key reagents), annealed, phosphorylated, and ligated into the BbsI sites of the pU6-BbsI-chiRNA plasmid (Gratz et al., 2013). Homology arms were PCR amplified and cloned into pHD-dsRed-attP (Gratz et al.,2014). Guide RNAs and the donor vector were co-injected into nosP>Cas9 attP embryos at the following concentrations: 250 ng/ml pHD-DsRed-attP donor vector and 20 ng/ml of each of the pU6-BbsI-chiRNA plasmids containing the guide RNAs (Rainbow Transgenics). Injected embryos were allowed to develop into larvae and crossed to wild type strains. The progeny of this cross was screened by a fluorescent fly microscope to allow for detection of positive KO/KI events by presence of DsRed.

Cloning of *Drosophila Gcna* transgene

PCR products were cloned into pENTR (Life Technologies) and swapped into pAHW, pAWG (attB added by Tony Harris) or pAFHW (Drosophila Gateway Vector Collection) using an LR reaction. Using this approach, we isolated clones corresponding to the *CG14814* cDNA (accession number BDGP:RE06257) transcripts.

Live imaging

3-5 day old males and virgin females were mated in mating cages containing grape juice (3%) agar plates with a little bit of wet yeast. The flies were allowed to lay eggs for 1-2 hrs at 25°C. Eggs were carefully collected and dechorionated by rolling them on double-sided tape pasted

on a slide. Dechorionated eggs were then mounted using oil and non-auto-fluorescent glue. Live imaging was conducted every 15 seconds using a Zeiss LSM800 microscope.

Fertility assays

0-2 day-old wild type males and virgin females of the genotype being tested were mated in mating cages with grape juice (3%) agar plates with a little bit of wet yeast. The flies were allowed to lay eggs for 48-72 hrs at 25°C before switching out the plates. Flies were allowed to lay eggs for a total of 7 days before eggs were counted.

Structured illumination microscopy (SIM) imaging and image processing

Ovaries were dissected according to standard protocol and mounted in Prolong Gold antifade reagent (Life technologies). Nikon N-SIM system (Nikon, Tokyo, Japan) equipped with a 100×/1.49 TIRF oil immersion objective lens (Nikon), the iXon + electron multiplying charged-coupled device camera (Andor) and an excitation laser unit of 405 nm, 488 nm, 561 nm and 640 nm (Coherent) was used for a superresolution optical imaging. Z-stacks of SIM optical sections were acquired with a 120 nm Z-step size. Image processing, including 3-dimensional reconstruction and colocalization analysis, were carried out using the NIS-Element Advanced Research software (Nikon).

Irradiation of flies

Adult flies were placed in a bottle for 24 hours and flipped out before exposing to 0 or 10 Gy from a cesium source. The progeny that survived to eclosion were counted and noted genotype. The ratio of homozygotes to heterozygotes was used to determine radiation sensitivity.

Hydroxyurea exposure

0-2 day-old wild-type and *Gcna*^{KO} female flies were collected and fed on wet yeast for 24 hrs. They were then starved for 16-18 hrs. Whatman paper was soaked in either 1% sucrose alone or 1% sucrose with 50mM Hydroxyurea. Flies were allowed to feed on sucrose with solvent or drug for 24 hours before being dissected and immunostained.

Scanning electron microscopy

Eggshells were mounted on SEM stubs and sputter coated with gold/palladium in a Cressington 108 auto sputter coater. Images were acquired on a Field-Emission Scanning Electron Microscope (ZeissSigma, Carl Zeiss, Thornwood, NY) at 10.0 kV accelerating voltage for WT embryos and 8.0 kV accelerating voltage for *Gcna*^{KO} embryos.

FISH

0-2 hour embryos were fixed according to "Immunofluorescence". FISH was performed on embryos according to Beliveau *et al* (2015). Embryos were washed once in the following: 1x PBS, 1x PBS + 0.1% Tween for 1 minute, 1x PBS + .5% Triton for 10 minutes, 1x PBS + 0.1% Tween for 1 minute, and .1N HCl for five minutes. Embryos were washed three times in 2X

SSC + 0.1% Tween (SSCT). Embryos were washed in 2X SSCT/50% formamide (Sigma) for 5 minutes. Embryos were incubated in 2X SSCT/50% formamide at 60°C for 20 minutes. Probes were prepared in solution of 10% dextrose, 2X SSC, 50% formamide and 30 pmol of oligopaint probe. Probes were added to the samples and denatured at 78°C for 2.5 minutes. Samples were incubated overnight at 42°C. Embryos were washed in 2X SSCT/50% formamide at 60°C and then room temperature. Embryos were washed in 0.2X SSC and mounted in Vectashield mounting medium + DAPI.

RNA sequencing

30 ovaries were dissected from *Gcna*^{KO} and control (*w*^{Berlin}) flies. There were three biological replicates produced from independent backcrosses of the KO into *w*^{Berlin} background for each sample. Qiagen miRNeasy Mini kit was used for RNA extraction and the RNA was sent for library preparation that selected for total RNA at McDermott Sequencing core at UTSW. The samples were sequenced in Illumina HiSeq 2500 cycle single-read platform. The sequencing reads were checked for quality using FastQC program (http://www.bioinformatics.babraham.ac.uk/projects/fastqc/). For analyzing differential gene expression, STAR aligner (version 2.5) (Dobin et al., 2013) was used to map the RNA-Seq reads to the Drosophila reference genome (genome assembly BDGP6.88) with an additional flag --outFilterMultimapNmax 100. TEtranscripts (Jin et al., 2015) was used to generate the read counts that mapped to TEs and genes. DESeq2 (Love et al., 2014) was used for differential expression analyses of TEs with a FDR of 5%.

DNA extraction and genotyping

A single fly from each genotype were ground and DNAzol and pelleted to clear debris. The DNA was then ethanol precipitated with 100% ethanol and incubated at -20°C for 20 minutes. Genotyping PCR was performed using the SapphireAmp fast PCR from Takara.

CHAPTER THREE
GCNA preserves genome integrity and fertility across species

Introduction

Early in the development of metazoans, primordial germ cells are set apart from somatic cells and undergo special programs to preserve genome integrity across generations. These programs include producing haploid gametes through meiosis, inducing and repairing programmed DNA double-strand breaks (DSBs), inhibiting transposable elements, and reprogramming chromatin to an epigenetic state that supports totipotency in the fertilized zygote (Kurimoto and Saitou, 2018; Tang et al., 2016). Facilitating these processes are a subset of germ cell-specific proteins that have been conserved across millions of years, including the DEAD-box helicase VASA, the RNA-binding protein NANOS, and the piRNA processing enzyme PIWI/Argonaute.

The recently identified Germ Cell Nuclear Acidic Peptidase (GCNA), also known as Germ Cell Nuclear Antigen or Acidic Repeat Containing (ACRC), has been conserved across 1.5 billion years of evolution. GCNA has remained tightly associated with sexual reproduction showing enriched expression within germ cells in both invertebrate and vertebrate species (Carmell et al., 2016). GCNA proteins contain an N-terminal acidic intrinsically disordered region (IDR) which is conserved structurally despite amino acid divergence. In most species, but not rodents, GCNA proteins also contain a C- terminal SPARTAN (SprT)-domain which

resembles a bacterial metalloprotease, a Zinc finger (ZnF), and an HMG box. Despite this modular domain structure, insights into GCNA function are lacking.

IDR-containing proteins have emerged as important players in cell biology, regulating phase transitions in a number of membrane-less organelles (Banani et al., 2017). In the nucleus, IDR proteins help form nucleoli, speckles, and Cajal bodies. All of these condensates are thought to be macromolecular assembly sites for protein-nucleic acid complexes that control chromatin structure, transcription, and various aspects of RNA processing. IDR proteins are also found in numerous germ cell-specific structures (Seydoux, 2018). For example, the IDR-containing MUT-16 protein phase separates to form mutator bodies in worms (Uebel et al., 2018). VASA also contains an extensive disordered region which contributes to its molecular behavior and function (Nott et al., 2015). Similarly, *C. elegans* MEG-3 and MEG-4 proteins bind to and phase separate RNA to form granules both *in vitro* and *in vivo* (Smith et al., 2016). MEG-3 and MEG-4 are GCNA family members, raising the possibility that GCNA itself may mediate essential germline functions through its IDR.

Potential insight into GCNA function comes from recent investigation into the functions of Spartan proteins for which the SprT-domain gets its moniker. Several independent groups have provided evidence that Spartan proteins specifically cleave DNA-protein crosslinks (DPCs) through their SprT protease domain (Lopez-Mosqueda et al., 2016; Stingele et al., 2016; Vaz et al., 2016). DPCs represent particularly insidious lesions that interfere with almost every chromatin-based process including replication, transcription, and chromatin remodeling (Stingele et al., 2017). The protease activity of Spartan appears highly regulated, and one major target of Spartan proteolysis is Spartan itself. Loss of Spartan in humans and

mice results in sensitivity to UV damage, progeroid-like phenotypes, and a predisposition to hepatocellular carcinoma, suggesting the protein plays an essential role in maintaining genome integrity (Davis et al., 2012; Mosbech et al., 2012). Within the germ line, the topoisomerase-like enzyme Spo11 forms DPCs to drive the formation of meiotic DSBs (Keeney et al., 1997). DPCs also occur during mitotic and meiotic DNA replication through the activity of topoisomerases. In addition, epigenetic reprogramming, including histone demethylation, creates cross-linking by-products like formaldehyde (Walport et al., 2012) that can result in DPC formation (Stingele et al., 2017). Inability to remove these DPCs would interfere with the faithful transmission of the genome over generations.

Here, we provide evidence that loss of *Gcna* results in genomic instability in *Drosophila*, *C. elegans*, zebrafish, and human germ cell tumors. GCNA acts to limit Spo11 activity in flies and prevents replication stress in flies and worms. Further analysis shows that GCNA functions in parallel to Spartan proteins within germ cells. Loss of *Gcna* results in the accumulation of DPCs in germ cells and early embryos. Genetic and transgenic analysis points to distinct roles for the IDR and SprT domains of GCNA. Together, these results reveal a new mechanism by which germ cells ensure the integrity of their genomes from one generation to the next.

Results

Drosophila Gcna mutants exhibit genome instability and chromosome segregation defects

Gcna exhibits enriched expression in germ cells across species (Carmell et al., 2016). We turned to *Drosophila*, *C. elegans*, and zebrafish as model systems in which to characterize the molecular function of GCNA family members. The *Drosophila* genome encodes for three potential GCNA orthologs (Figures 3.1A,B; 3.2). Only null mutations in *CG14814* (hereafter called *Gcna*, Fig 3.1B), resulted in overt phenotypes, while the others appeared viable and fertile (Figure 3.2A-E). Homozygous $Gcna^{KO}$ mutant females initially laid eggs but stopped after approximately one week. Many of the embryos derived from these eggs exhibited maternal-effect lethality (Figure 3.2F). Fixed and live-cell imaging experiments revealed that loss of maternal Gcna resulted in numerous mitotic defects during early embryogenesis including chromosome tangling, micronucleus formation, nuclear fusion, chromosome segregation defects, and disruption of cell-cycle synchrony (Figure 3.1C-E).

The few adult, F1 progeny from *Drosophila* $Gcna^{KO}$ mutant females appeared sickly and sub-fertile. Of these, four percent displayed bilateral gynandromorphism (Figures 3.1F; 3.2G) a rare phenotype caused by X chromosome loss during the early embryogenesis (Janning, 1978). Chromosome loss was not X chromosome-specific as shown by fluorescent *in situ* hybridization (FISH). In control female embryos, two discrete X-chromosome foci (359-bp repeat probes) and two chromosome 2 foci ($AACAC_{(n)}$ probes) were observed in dividing nuclei, as expected for a diploid cell (Figure 3.1G). By contrast, embryos from $Gcna^{KO}$ mutant females displayed X-chromosome bridges and second chromosome

missegregation and polyploidy (Figure 3.1G). Similar chromosomal phenotypes were also observed in *Gcna* mutant ovaries (Figure 3.2H).

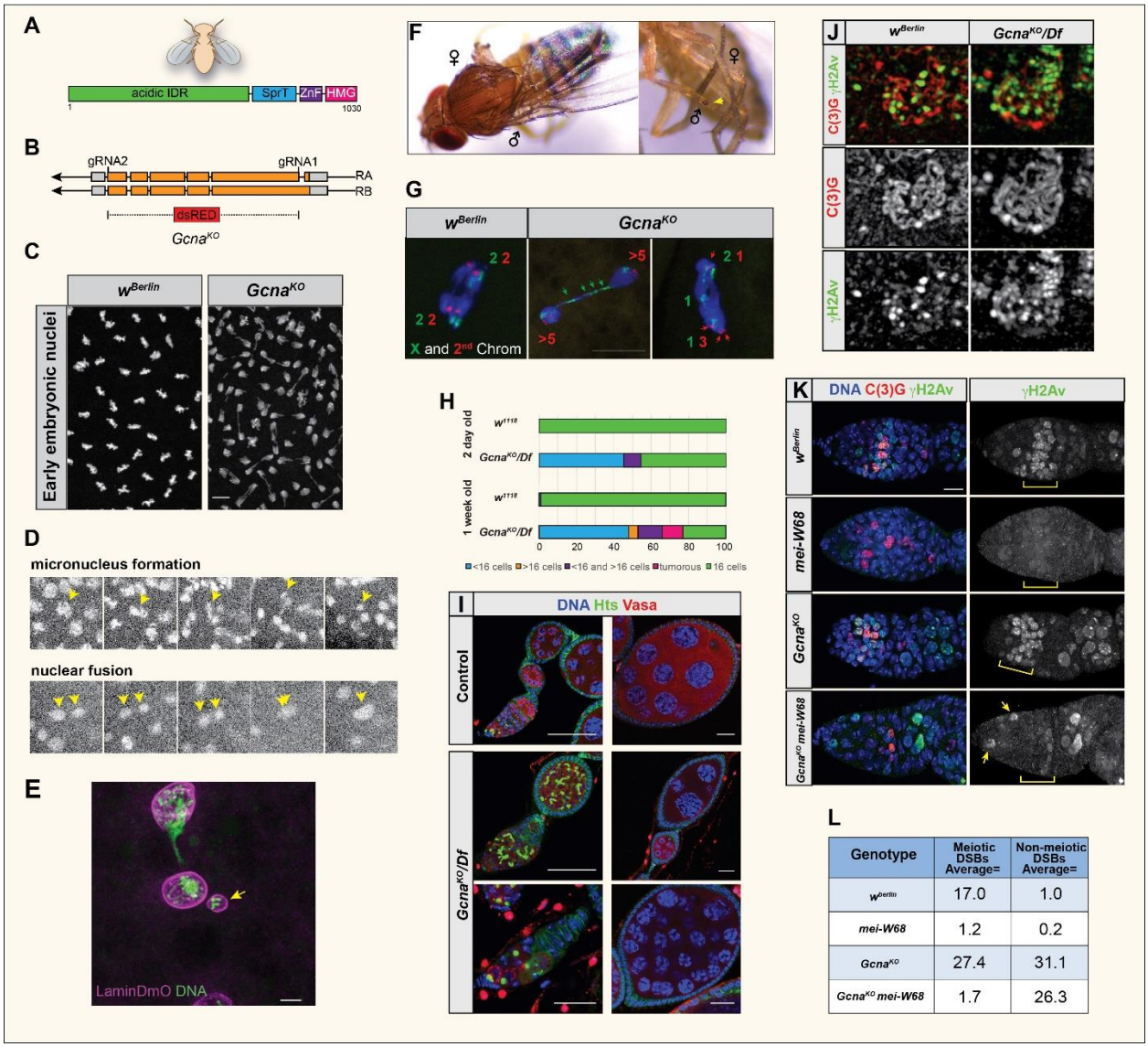

Genotype	Meiotic DSBs Average=	Non-meiotic DSBs Average=
w^Berlin	17.0	1.0
mei-W68	1.2	0.2
Gcna^KO	27.4	31.1
Gcna^KO mei-W68	1.7	26.3

Figure 3.1. Loss of *Gcna* results in chromosome instability in *Drosophila*. (**A**) Domain organization of the *Drosophila* Gcna protein. (**B**) *Drosophila Gcna* gene locus showing the two isoforms and design of the $Gcna^{KO}$ allele with insertion of a dsRED cassette. UTRs in grey, exons in orange. (**C**) DAPI staining of control (w^{Berlin}) and $Gcna^{KO}$ (maternal null) embryos reveals mitotic defects caused by loss of maternal *Gcna*. Scale bar represents 10µM.**(D)** Still images from movies of $Gcna^{KO}$ maternal-null embryos carrying a *HistoneH2Av-mRFP* transgene to visualize chromosomes. Yellow arrowheads indicate micronucleus formation (top) and nuclear fusion event (bottom). **(E)** Early *Gcna* maternal mutant *Drosophila* embryo stained for Lamin Dm0 (magenta) and DNA (green) to show that a nuclear envelope forms around a micronucleus (yellow arrow). Scale bar represents 5 µm. (**F**) Gynandromorph phenotypes in progeny of $Gcna^{KO}$ females. Left, note the line of dark and light pigmentation bisecting the thorax, reflecting the presence or absence of the *yellow* marker carried on one of the X chromosomes. Right, sex combs are seen on one forelimb (yellow arrow) but are missing from the other, reflecting adoption of male and female fates respectively. (**G**) Embryonic nuclei from control (w^{Berlin}) and $Gcna^{KO}$ mutant females were labeled with FISH probes to the X (green) and second (red) chromosomes. The green and red numbers refer to number of X and second chromosome-specific foci observed in each half of the dividing nuclei. Controls show chromosomes dividing equally into daughter cells. $Gcna^{KO}$ cells have aberrant chromosome numbers and lagging chromosomes (green arrows). Scale bar represents 5 µm. (**H**) Quantification and **(I)** corresponding images of *Drosophila* ovarian phenotypes. Hts marks the fusome; Vasa marks germ cells. Control (w^{1118}) ovarioles contain the expected 16-cell cysts. $Gcna^{KO}/Df$ ovarioles have many cysts with abnormal numbers of cells, as well as tumors. The frequency of these phenotypes worsens with age. Scale bars represent 20 µm. (**J**) SIM images of w^{Berlin} and $Gcna^{KO}$ mutant meiotic nuclei stained for synaptonemal complex marker C(3)G (red) and DNA damage marker γH2Av (green).

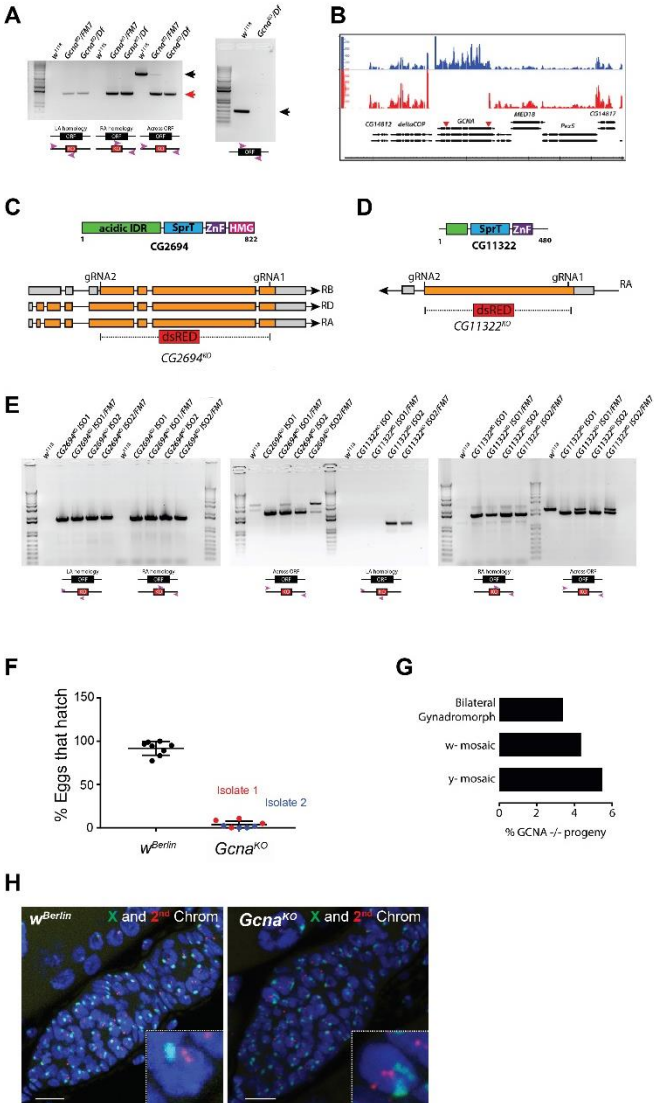

Figure 3.2. Loss of *GCNA* results in chromosome instability. (**A**) PCR verification of the *Drosophila* *Gcna*^{KO} mutation using primers indicated by pink arrowheads. Black arrow points to wild-type product; red arrow to mutant product. LA= left arm; RA= right arm. (**B**) Reads from RNA-Seq showing that *Gcna*^{KO} homozygotes do not express *Gcna* (WT, top, blue; mutant, bottom, red). (**C, D**) Protein domain structure and gene organization of *Gcna*-related loci in *Drosophila*. (**C**) *CG2694*, (**D**) *CG11322*. (**E**) PCR confirmation of knockout alleles using primers indicated below. (**F**) Quantification of embryonic viability of egg derived from control and two independent isolates of the *Gcna*^{KO}. n > 500. (**G**) Quantification of chromosome loss phenotypes in *Gcna*^{KO} animals that survive to adulthood. Bilateral gynandromorphs exhibit chromosome loss at the first divisions; *w* and *y* mosaics result from chromosome loss at later cell divisions. (**H**) FISH for the X (green) and second (red) chromosomes performed on *w*^{Berlin} control and *Gcna*^{KO} mutant ovaries shows normal karyotypes in control and altered karyotypes in the mutant. Inset shows a single germ cell nucleus. Scale bars represent 10 µm.

Drosophila Gcna mutant ovaries exhibit increased DNA damage

Loss of fly *Gcna* also resulted in specific ovarian phenotypes (Figure 3.1H,I; 3.3A-D). For example, many *Gcna* mutant egg chambers deviated from the normally-invariant number of 16 germ cells per cyst. In aged flies, this phenotype became more penetrant. Labeling of ring canals, which form from arrested cleavage furrows, and the cell death marker Cleaved Caspase 3 suggested that the counting defects arose from abnormal cell divisions and loss of cell-cycle synchrony (Figure 3.3A, data not shown). We also observed defects in differentiation and delayed oocyte specification (Figure 3.3B,C).

To test whether *Gcna* regulates meiosis in *Drosophila*, we examined γH2Av, a marker of DNA damage (analogous to γH2AX), and C(3)G, a synaptonemal complex (SC) protein (Jang et al., 2003; Page and Hawley, 2001). In control ovaries, the SC and γH2Av foci were first observed in region 2A of the germarium, as previously described (Jang et al., 2003). In *Gcna* mutant germaria as revealed by structured illumination microscopy (SIM), the SC formed normally; however, γH2Av foci appeared larger and more abundant (Figure 3.1J-L).

In control germaria, DSBs are rapidly repaired. However, in *Gcna* mutant germ cells, γH2Av staining extended into early egg chambers (Figure 3.1K). Expression of a *p53* reporter, which correlates with DNA damage (Lu et al., 2010; Wylie et al., 2014), was also expanded (Figure 3.3D). To determine if the persistent DNA damage reflects a defect in DSB repair, we asked whether *Gcna* mutations disrupt homologous recombination (HR). Unlike HR-defective *Rad51* and *Rad54* mutants, which exhibit dorsal appendage defects in 50-60% of their eggs (Abdu et al., 2003; Ghabrial et al., 1998; Staeva-Vieira et al., 2003), only 4-8% of *Gcna* mutant eggs have this phenotype (Figure S2E; n>200 eggs from multiple lays). *Gcna* mutant meiotic

nuclei also have more γH2Av foci than HR pathway mutants (Figure 3.3F; (Jang et al., 2003)). *Gcna* mutant flies also do not display whole body sensitivity to irradiation (IR, Figure 3.3G), unlike *Rad51* and *Rad54* mutants (Ghabrial et al., 1998; Staeva-Vieira et al., 2003). Together with our observation that meiotic nondisjunction rates did not vary between controls and $Gcna^{KO}$ homozygotes (Figure 3.3H), these results suggest that Gcna likely does not play an essential role in HR-mediated repair in *Drosophila*.

We next considered that the excess γH2Av foci in *Gcna* mutant ovaries resulted from disruption in spatial or temporal regulation of meiotic DSB induction by Spo11. If correct, this model would predict that loss of either *spo11,* named *mei-W68* in *Drosophila* (McKim and Hayashi-Hagihara, 1998), or *mei-P22*, a gene needed for targeting mei-W68 (Liu et al., 2002), would suppress *Gcna* mutant phenotypes. Loss of either *mei-W68* or *mei-P22* functions in the *Gcna* mutant background resulted in a dramatic suppression of the extra meiotic DSBs in region 2A (Figures 3.1K,L; 3.3I). In these double mutants, however, we still observed γH2Av staining in pre-meiotic and later germ cells suggesting a subset of breaks arise independently of the meiotic program. In addition, neither *mei-P22* nor *mei-W68* mutations suppressed other phenotypes associated with loss of *Gcna*, including the germ-cell counting defects and maternal-effect semi-lethality. Thus, it appears that GCNA functions in flies to maintain various aspects of genome integrity during both meiotic and mitotic divisions.

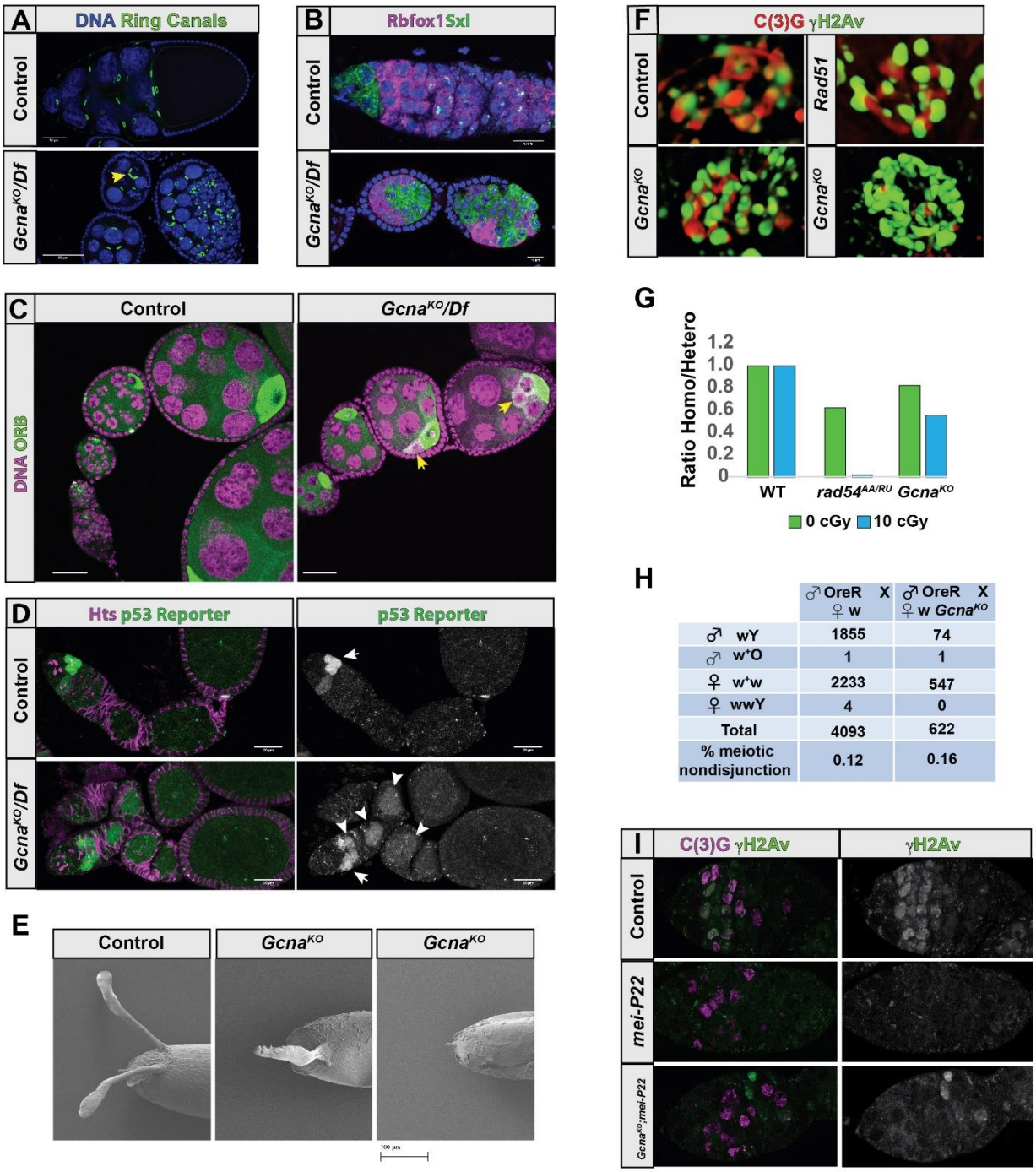

	♂ OreR X ♀ w	♂ OreR X ♀ w *Gcna*^{KO}
♂ wY	1855	74
♂ w$^+$O	1	1
♀ w$^+$w	2233	547
♀ wwY	4	0
Total	4093	622
% meiotic nondisjunction	0.12	0.16

Figure 3.3. Loss of *Gcna* results in oogenesis defects in *Drosophila*. (**A-D**) *Gcna* loss leads to "counting defects" and cysts with too few or too many cells. Control and *Gcna*^{KO}*/DF* ovaries are stained for (**A**) DNA (blue) and ring canals marker, Hts-RC (green). Yellow arrowhead points to oocyte with only three ring canals. (**B**) Rbfox1 (magenta) and Sxl (green) show an expansion of early cell fates in *Gcna* ovaries, (**C**) DNA (magenta) and Orb (green). Yellow arrowheads point to germ cells with abnormal accumulation of Orb, (**D**) Hts (magenta) and a p53 reporter (green). White arrowheads point to germ cells with aberrant accumulation of p53. (**E**) *Gcna* mutant eggs exhibit dorsal-ventral patterning defects similar to DNA repair-defective mutants. Scanning EM images of control eggs shows the 2 dorsal appendages; *Gcna*^{KO} eggs can have normal (not shown), fused, or missing appendages.

C. elegans gcna-1 mutants exhibit genomic instability in later generations

In parallel with the *Drosophila* experiments described above, we collaborated with the Yanowitz lab to make a null mutation in the *C. elegans Gcna* homolog, CELE_ZK328.4 (now called *gcna-1*) (Figure 3.4A,B). A previous large-scale RNAi screen noted that *gcna-1* knockdown resulted in a very mild High Incidence of Males (HIM) phenotype (Colaiacovo et al., 2002), which is indicative of X chromosome nondisjunction (Hodgkin et al., 1979). Our CRISPR/Cas9-induced null allele confirmed this mild HIM phenotype, which is exacerbated by growth at higher temperature (25°C) and at later generations (Figure 3.4C). Moreover, we found that loss of *gcna-1* gives rise to a mortal germ line (MRT) phenotype characterized by transgenerational loss of fecundity and vitality, marked by reduced lifespan, decreased mobility, and loss of fertility in later generations (Figure 3.4D; Figure 3.5A,B).

Whereas wild-type worms contain two U-shaped germlines filled with developing oocytes that ultimately arrest at diakinesis of prophase I with 6 bivalent chromosomes, late generation *gcna-1* mutant germ lines showed a range of phenotypes, from near wild-type to severely runty germ lines (Figure 3.5C). Diakinesis nuclei of late generation *gcna-1* mutant animals showed chromosomal abnormalities with 4 – 9, often irregularly-shaped, DAPI-stained bodies (Figure 3.4E), indicative of chromosome fusions and defects in crossover formation (Dernburg et al., 1998; Hillers et al., 2017). Multiple independent lines began to produce excessive male offspring in the several generations before the onset of sterility. In these populations, all worms assayed presented with a consistent karyotype of 5 DAPI-positive bodies suggesting they may have contained X:autosome fusion chromosomes. Similar to the fly embryo, we observed chromosome bridges and chromosomal fragments in *gcna-1* mutant

germ cells (Figure 3.4F). Together, the fly and worm mutant phenotypes indicate that loss of *Gcna* function disrupts reproductive success and chromosome stability across species.

Excessive DNA damage during meiosis was not obvious in *C. elegans gcna-1* mutants (Figure 3.5D). By crossing *gcna-1* into a *spo-11* mutant background and exposing worms to the DSB-inducing agent IR, we were able to see similar accumulation of RAD-51 in *spo-11* and *gcna-1;spo-11* (Figure 3.5E), suggesting that early steps in HR are normal in *gcna-1* mutant animals, as they are in *Drosophila Gcna* mutants. Consistent with this observation, *gcna-1* mutant worms did not show increased IR sensitivity (Figure 3.5F). Nevertheless, RAD-51 foci were present in the pachytene nuclei of the unirradiated *gcna-1;spo-11* mutant controls (Figure 3.4G) suggesting DNA damage arose during either mitotic divisions of germ cells or meiotic S phase. This "carry through" damage can induce meiotic crossover (CO) formation as seen by a decrease in univalent chromosomes in *gcna-1;spo-11* compared to *spo-11* mutant worms (Figure 3.4H). Together with the *Drosophila* experiments, these findings indicate that while GCNA plays species-specific roles in the regulation of Spo11 activity during meiosis, loss of *Gcna* function leads to the accumulation of Spo11-independent DSBs within both *Drosophila* and *C. elegans* germ cells.

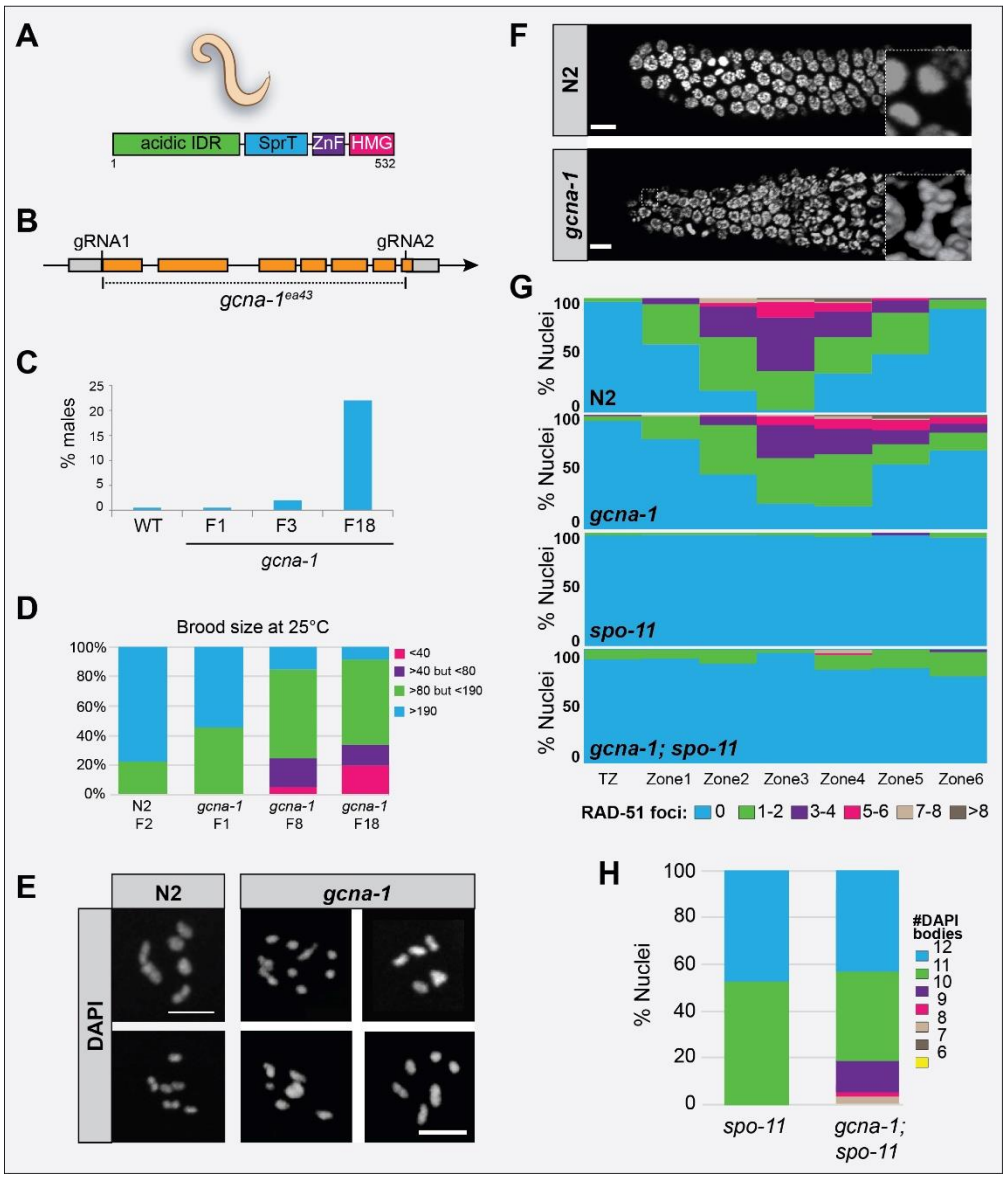

Figure 3.4. Loss of *gcna-1* results in genomic instability in *C. elegans*. (**A**) Domain structure of *C. elegans* GCNA-1 protein. (**B**) The *C. elegans gcna-1* locus detailing the design of the *gcna-1(ea43)* allele. (**C**) The HIM phenotype increases over generations (n=12 parental worms for N2 (wild type control) and n= 21, 21, 34 for *gcna-1* F1, F3, and F18, respectively). (**D**) *gcna-1* mutant worms exhibit decreases in brood size with successive passaging (n=12 parental worms for wt, and 34 each for *gcna-1* F1, F8, and F18). (**E**) DAPI staining of diakinesis nuclei from control (N2, wild type) and *gcna-1* mutants. Controls showed the expected 6 DAPI^{+} bivalents; *gcna-1* mutant nuclei contained mixtures of bivalents, univalents, and fused chromosomes. Scale bars represent 5 µm. (**F**) Mitotic germ cells from *gcna-1* mutants exhibit chromosome bridges as seen by DAPI-stained DNA. Insets are examples of nuclei in anaphase. Scale bars represent 20 µm. (**G**) Quantification of meiotic (leptotene through onset of diplotene) RAD-51 foci in *N2, gcna-1, spo-11*, and *gcna-1;spo-11* mutant *C. elegans* germ lines (n = 3 germ lines/ genotype). (**H**) Quantification of DAPI positive bodies in diakinesis-stage, -1 oocytes of *C. elegans* (*spo-11*, n= 20; *gcna-1;spo-11*, n=42). In collaboration with the Yanowitz lab.

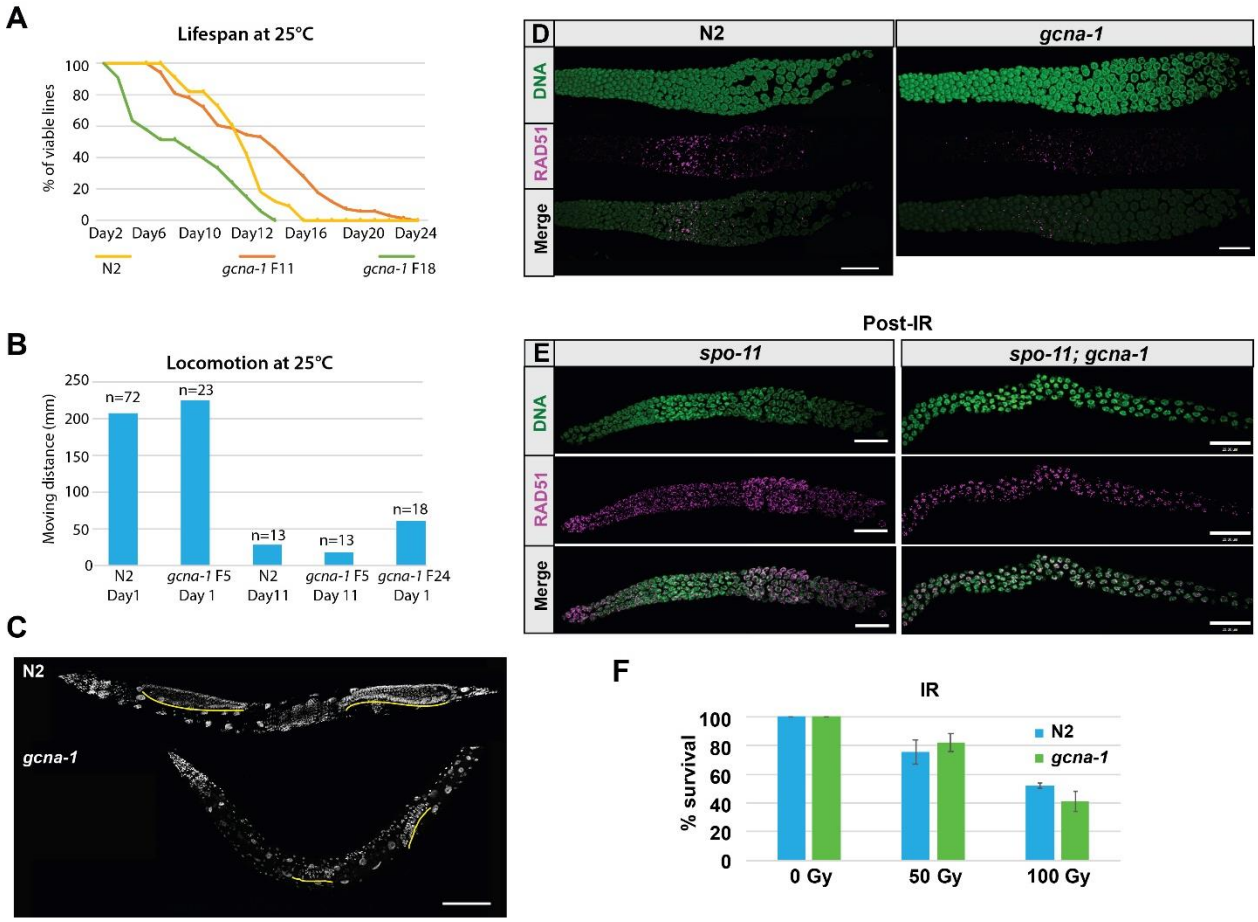

Figure 3.5. Loss of *gcna* results in a mutator phenotypes in worms. (**A-C**) Lifespan, healthspan, and fertility of *gcna-1* mutant *C. elegans* decrease with serial passaging. (**A**) Kaplan-Meier plot of control and *gcna-1* mutant at indicated generations. (**B**) Quantification of locomotion in control and *gcna-1* mutant *C. elegans*. (**C**) DAPI staining of control (N2) and late generation *gcna-1* mutant worms showing a reduction in in gonad size (yellow lines).(**D-F**) *gcna-1* mutants show a reduction in meiotic RAD-51 staining but are not defective in responding to DNA damage. (**D**) N2 control and *gcna-1* mutants stained for DNA, green and RAD-51, magenta. Fewer meiotic RAD-51 are seen in *gcna-1* mutant gonads. (**E**) *gcna-1* mutants accumulate RAD-51 as expected after exposure to gamma irradiation as shown by comparing irradiated *spo-11* (no meiotic DNA damage) and *gcna-1;spo-11* mutants. (**F**) Viability of N2 and *gcna-1* mutant embryos after exposure of mothers to increasing doses of IR. In collaboration with the Yanowitz lab.

Replication stress as a source of DNA damage in Drosophila and C. elegans

One source of Spo11-independent DSBs are transposable elements (TE) whose mobilization creates DSBs that can induce crossovers (Soper et al., 2008). We carried out

experiments to determine if GCNA controls TE surveillance (Figure 3.6). We saw a modest increase in TE expression in worms (Figure 3.6A) which suggested a potential role for GCNA in the TE surveillance pathway governed by piRNAs/PIWI. However, *gcna-1* mutations were synthetic sterile with *prg-1/*PIWI mutations (Figure 3.6B), arguing that GCNA acts in parallel to the canonical TE surveillance pathway. Consistent with these observations, *Gcna* mutant flies did not show altered expression or localization of Aubergine, a piRNA pathway component (Figure 3.6C). Transcriptomic analyses identified an approximate 2-fold increase in expression of telomere-associated TEs and a concomitant decrease in metabolic genes in *Drosophila Gcna* mutants (Figure 3.6D-H), raising the possibility that cellular stress pathways may be activated in *Gcna* mutants. These cross-species studies hint at mild effects on TE regulatory pathways but are unlikely to explain the substantial increase in DNA damage and phenotypic consequences observed in *Gcna* mutants.

We next considered the possibility that *Gcna* mutants experience replicative stress, which is a major cause of endogenous DSBs, chromosome segregation defects, and cell cycle disruption (Magdalou et al., 2014; Zhang et al., 2018). To determine if GCNA participates in replicative repair, we took advantage of an established assay in worms to interrogate microsatellite repeat stability in collaboration with the Yanowitz lab. The DEAD-box helicase *dog-1/FANCJ* is the only known gene required for replication of G-quadraplex-like structures in worms (Kruisselbrink et al., 2008) and is required for accurate replication through GC-rich DNA (Youds et al., 2008). Accordingly, *dog-1* mutations exhibit microsatellite repeat instability (MSI), as readily seen in a PCR-based assay of repeats at the *vab-1* locus ((Youds et al., 2008); Figure 3.7A). Whereas *gcna-1* mutation did not exhibit repeat instability on its

own, it strongly enhanced *dog-1* (Figure 3.8A). This result is consistent with a role for GCNA in promoting replicative repair and/or replication restart.

When replication forks stall at DNA lesions or aberrant DNA structures, increased stretches of single-stranded DNA (ssDNA) form, which can be visualized as nuclear punctae of RPA (replication protein A), the major single-strand DNA binding protein in cells. In *Drosophila* germ cells, we observed a disruption of RPA expression and localization within *Gcna* mutant ovaries. $Gcna^{KO}$ mutant germ cells displayed discrete RPA nuclear foci that were rarely observed in controls (Figure 3.8B,C; 3.7B). Within *Gcna* mutant ovaries, these punctae were present in both mitotic germ cells within germaria and in endocycling nurse cells.

We also tested whether *Drosophila Gcna* mutant germ cells were sensitive to hydroxyurea (HU), an agent that limits the dNTP pools, causing replication fork stalling and DNA damage, particularly in mutants that already suffer from replication stress. Upon HU treatment, *Gcna* mutant germaria accumulated many more γH2Av foci within mitotically active cells relative to controls, indicating that loss of GCNA makes germ cells more sensitive to replicative stress (Figure 3.8D). In the associated manuscript, the authors found the *gcna-1* mutant worms were also mildly sensitive to HU (Davis et al., 2019). Taken together, these results support a potential role for GCNA in promoting replicative repair across species.

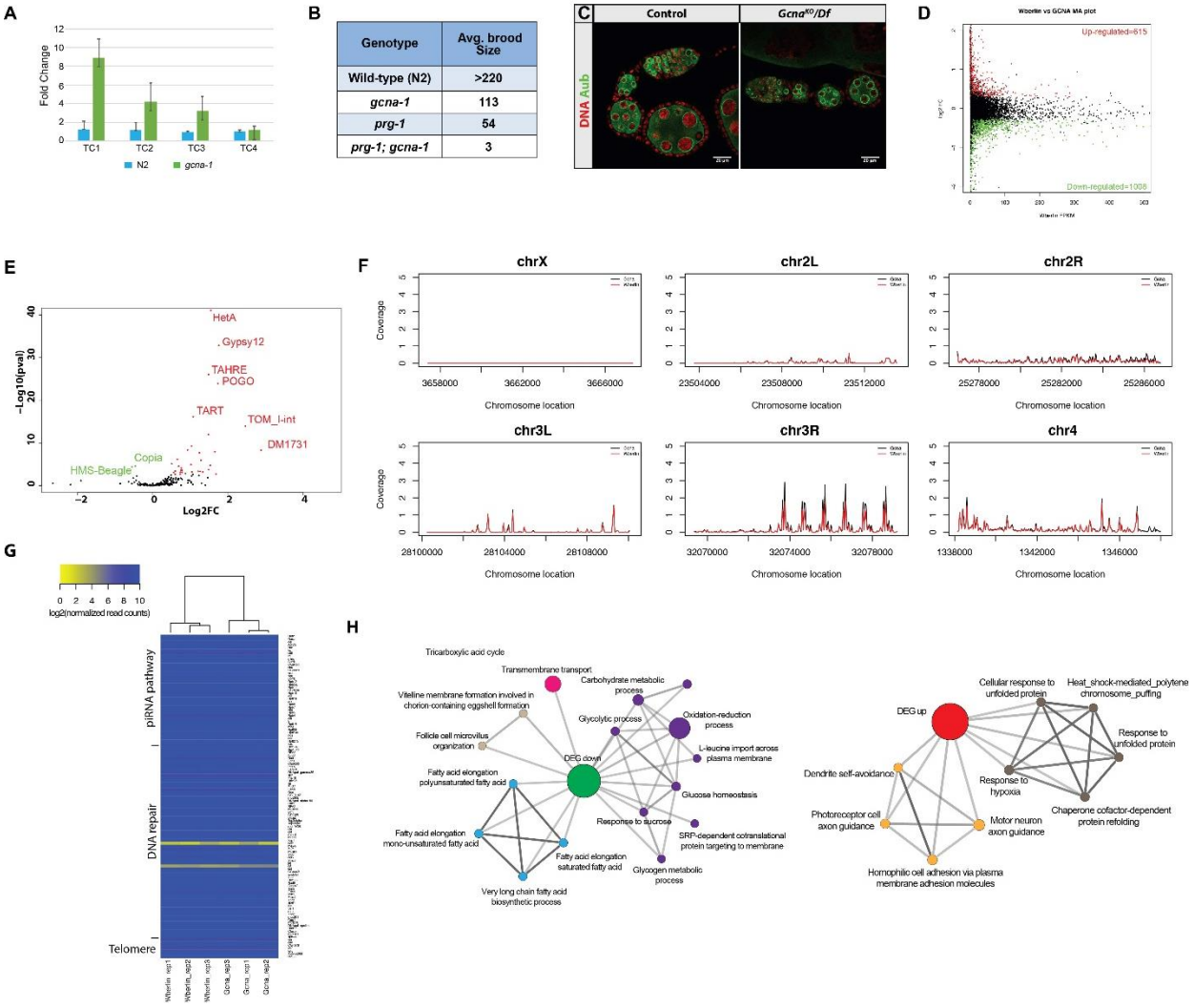

Figure 3.6. GCNA regulates transposable element (TE) expression but functions independently from the piRNA pathway. (**A**) Quantification of TE expression in *C. elegans* N2 and *gcna-1* mutants. (**B**) Comparison of brood sizes of N2 (n=10), *gcna-1* (n=10), *prg-1* (n=10), and *prg-1; gcna-1* (n=20) mutant worms shifted from 20°C to 25°C as young L4 larvae. The synergistic effect seen in *prg-1;gcna-1* suggests these genes function in parallel pathways to control fertility. (**C**) Expression of the PIWI-family protein Aubergine is unaltered in *Gcna*^{KO} germ cells. Control and *Gcna*^{KO}*/DF* ovaries stained for DNA (blue) and Aubergine (Aub) (Red). (**D**) MA plot comparing gene expression in *Gcna*^{KO} and *w*^{Berlin} ovaries. (**E**) Volcano plot comparing TE expression in a *Gcna*^{KO} and *w*^{Berlin} ovaries. (**F**) Telomere visualization for all *Drosophila* chromosomes using average read density from *Gcna*^{KO} (black) and *w*^{Berlin} (red) samples. (**G**) Heat map comparing expression of 127 piRNA pathway, DNA repair, and telomere maintenance genes between control samples and *Gcna* mutant ovaries. (**H**) GO analysis of the genes that exhibit down-regulation or up-regulation in a *Gcna*^{KO} background.

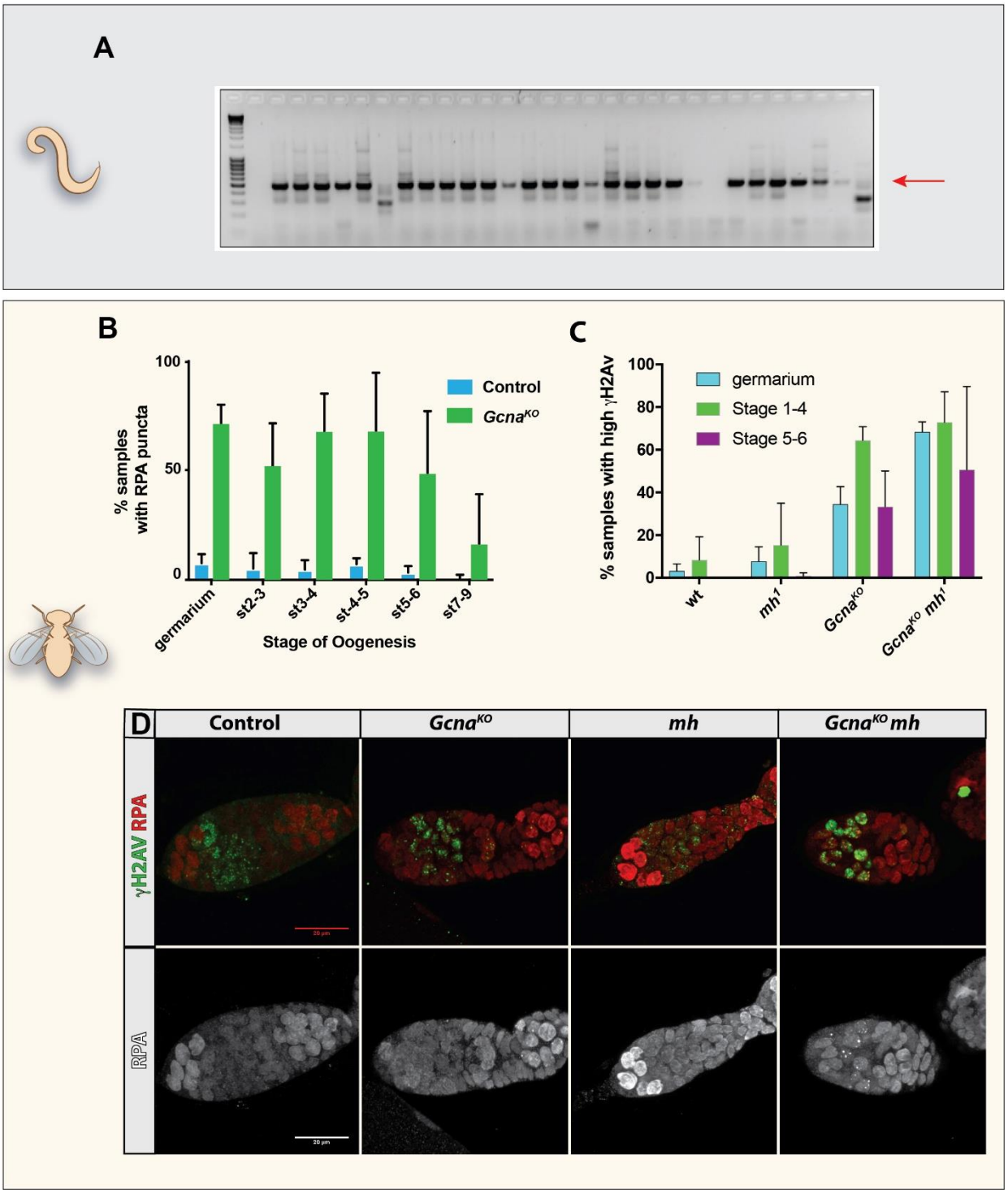

Figure 3.7. *Gcna* mutant worms and flies show hallmarks of replicative DNA damage. (**A**) Representative image of a gel from the dog-1 assay showing PCR amplification of of a GC-tract in the *vab-1* locus. Arrow indicates the expected size in control animals. Smaller bands indicate changes in microsatellite repeat lengths. (**B-D**) *Gcna* mutant *Drosophila* show increased markers of DNA damage. (**B**) Percent of control and *Gcna* mutant germline cysts at indicated stages of development that contain RPA foci. (**C**) Percent of control, *Gcna*, *mh*, and *Gcna mh* mutant germline cysts at the indicated stages with high levels (>25 foci) of nuclear γH2Av. (**D**) Representative images of control, *Gcna*, *mh*, and *Gcna mh* mutants stained for RPA (red) and γH2Av (green). In collaboration with the Yanowitz lab.

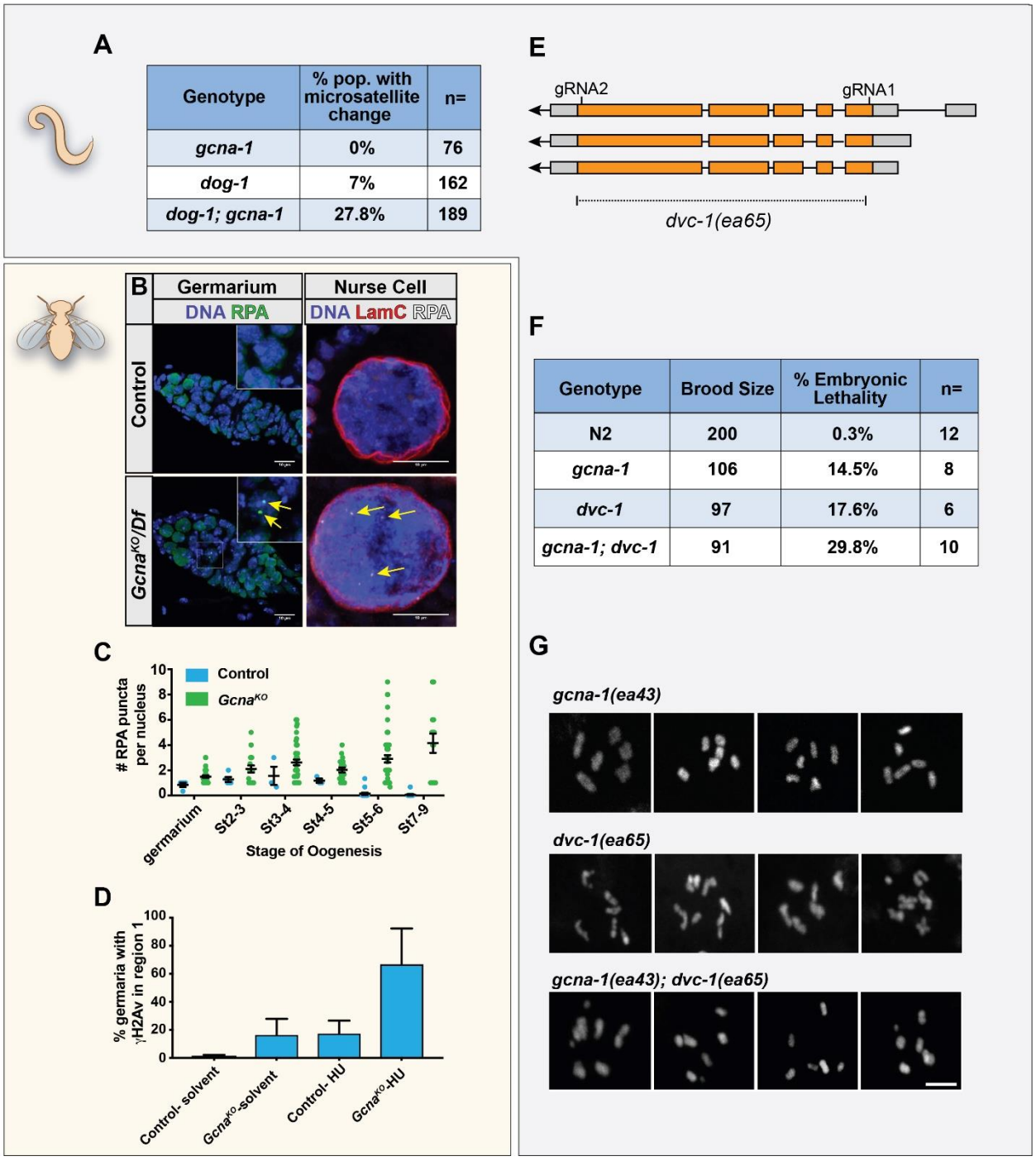

Figure 3.8. *GCNA* mutant germ cells experience replication stress. (**A**) Frequency of microsatellite repeat length changes within the *C. elegans vab-1* locus. (**B-C**) RPA foci (yellow arrows) accumulate in *Drosophila* $Gcna^{KO}$ germ cells. (**B**) Control and $Gcna^{KO}$*/Df* germaria (left) and nurse cell nuclei (right) stained for DNA (blue), RPA (green), and Lamin C (red) as indicated. Scale bars represent 10 µm. (**C**) Quantification of RPA punctae per nucleus. (**D**) Quantification of γH2Av foci in region 1 of the *Drosophila* germarium in control and $Gcna^{KO}$ mutant germaria in response to HU treatment. (**E**) The *dvc-1/Spartan* locus of *C. elegans* showing the strategy for creating a complete null, *dvc-1(ea65)*. (**F**) Brood analysis (total viable adult offspring) and embryonic lethality associated with N2, *dvc-1* and *gcna-1* single mutants, and *dvc-1;gcna-1* double mutant worms. (**G**) Examples of DAPI-stained, diakinesis oocytes from *dvc-1*, *gcna-1*, and *dvc-1; gcna-1* mutant germ cells show chromosome fragmentation in the double mutant. Scale bars represent 5 µm. In collaboration with the Yanowitz lab.

GCNA and Spartan act independently

DNA-protein crosslinks are a significant source of replicative stress (Vaz et al., 2017). GCNA is a Spartan family member, whose namesake removes DPCs (Stingele et al., 2016; Vaz et al., 2016). To determine whether GCNA has a similar function and/or acts together with Spartan, we crossed *Gcna* mutations into *Spartan* mutant backgrounds. In worms, Spartan is encoded by *dvc-1* (DNA damage-associated VCP/p97 Cofactor homolog). The previously described allele is a partial truncation that functions as a mutator, is slow growing and difficult to maintain (Stingele et al., 2016). We generated a full deletion allele, *dvc-1(ea65)* and maintained the stock as a balanced heterozygote. (Figure 3.8E). *dvc-1(ea65)* homozygotes conferred the reduced brood sizes (Figure 3.8F) described for *dvc-1(ok260)*. While *dvc-1* and *gcna-1* have near similar effect on brood size, *gcna-1;dvc-1* showed an additive effect, almost doubling embryonic lethality (Figure 3.8F; n>6 broods/ genotype, 3-way Kruskal-Wallis Test, $p<0.05$). Similarly, diakinesis nuclei of *dvc-1(ea65)* F3 homozygous animals contain aberrant chromosome numbers and morphologies that were further exacerbated by loss of *gcna-1* (Figure 3.8G). In *dvc-1* single mutants, chromosome fusions and fragments were seen in 33% and 14% of nuclei, respectively (n= 21; note that some nuclei have both fusions and fragments). In the *gcna-1;dvc-1* double mutants, the frequency of fusions was not statistically different (n= 26; Chi-square, $p>0.1$) yet chromosomal fragments were much more common (62% of nuclei; Chi-Square, $p < 0.001$). These results suggest that GCNA-1 acts independently of DVC-1 to ensure genomic stability.

For *Drosophila*, the Spartan homolog, *maternal haploid* (*mh*), helps maintain paternal chromosome integrity during early embryogenesis (Delabaere et al., 2014). The number of

eggs laid per female appeared comparable for *mh* and *Gcna* single mutants and *Gcna mh* double mutants. Of these embryos, 11% from *Gcna* mutant females (n=299) and 1.4% from mh^1 mutant females (n=444) hatched, while none of the embryos from *Gcna mh* double mutants (n=296) completed embryogenesis. Ovaries of *mh* mutants looked comparable to controls, whereas ovaries from *Gcna mh* double mutants exhibited increased γH2Av and RPA foci relative to control and single mutants (Figure 3.7C,D). These results suggest that Gcna and Mh likely act in parallel to limit DNA damage in the *Drosophila* germline, consistent with our worm data that Spartan and GCNA-1 act independently. These data raise the possibility that GCNA may have an independent role in clearing a subset of DPCs.

Loss of Gcna results in an accumulation of DPCs

We used the rapid approach to DNA adduct recovery (RADAR) coupled with SDS-PAGE and silver staining to evaluate whether GCNA influences DPC levels within *Drosophila* ovaries and early embryos (Figure 3.9A) (Kiianitsa and Maizels, 2013). We observed a modest, but consistently elevated, level of DPCs in the Gcna mutant ovaries and early embryos compared to controls (Figure 3.9B).

To identify proteins that formed DPCs, we analyzed the RADAR samples using mass spectrometry (Figure 3.10A). A number of proteins formed DPCs specifically in Gcna mutant embryos or ovaries, or both; these included Histone H2B, Topoisomerase 2 (Top2), SSRP1, MCM3 and Fibrillarin. These proteins were not detected in the wild-type samples although other proteins were, pointing to the specificity of the described effects. We repeated the RADAR assay on isolated nuclei from Drosophila embryos and found an enrichment of

specific DPCs in *Gcna* mutant samples (Figure 3.9C). The increased levels of Top2 and MCM protein DPCs in the *Gcna* mutant drew our attention. Top2 decatenates supercoiled DNA, while the MCM complex unwinds DNA in front of the replication fork. To begin to test the functional interactions between Gcna and these proteins, we immunoprecipitated a tagged form of Gcna from S2 cells and performed mass spectrometry (Figure 3.9D). Several, but not all, proteins found in DPCs in *Gcna* mutants also physically interact with Gcna protein. These included Top2, as well as multiple components of the MCM complex. These results further link GCNA with regulation of replication in germ cells and early embryos.

To characterize how *Gcna* loss affects the interacting proteins, we examined Top2 expression and localization (Figure 3.9E). In control embryos, Top2 localized to metaphase chromosomes, as previously reported (Tang et al., 2017). Low levels of cytoplasmic Top2 were also evident. By contrast, *Gcna* mutant embryos displayed a redistribution of Top2, with higher levels on metaphase chromosomes and decreased cytoplasmic localization. Gcna mutant egg chambers also exhibited more nuclear Top2 punctae (Figure 3.10B-D). This redistribution occurred independent of Top2 expression levels which were unchanged in *Gcna* mutants (Figure 3.10E). Finally, similar increases in chromosome-associated Top2 were observed in worm *gcna-1* mutant germ cells (Figure 3.9F), indicating that loss of *Gcna* results in increased accumulation of nuclear Top2 across species. Thus, we have demonstrated that GCNA both interacts with and impacts the localization of proteins that become associated with DPCs when *Gcna* function is impaired.

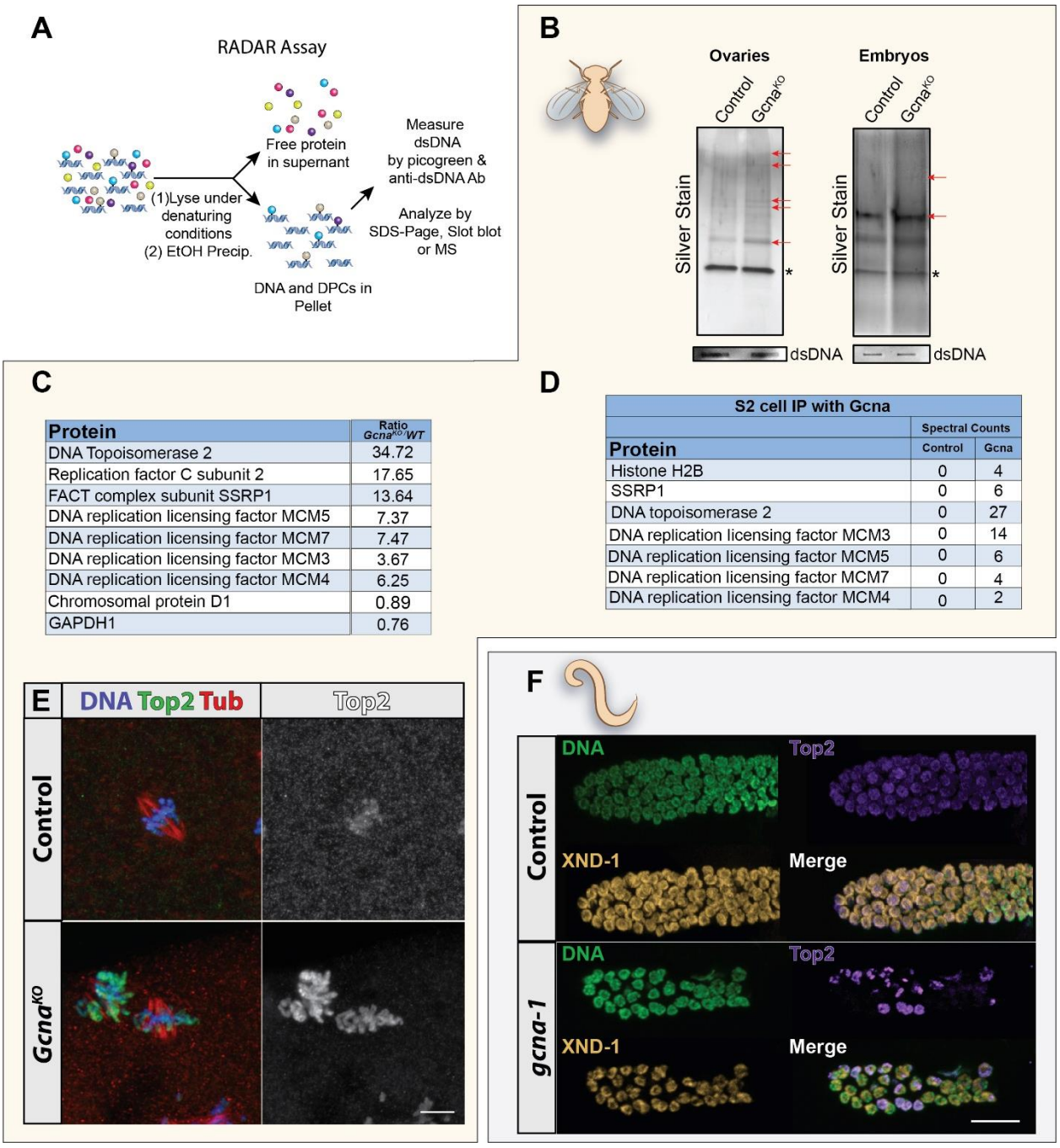

Protein	Ratio $Gcna^{KO}/WT$
DNA Topoisomerase 2	34.72
Replication factor C subunit 2	17.65
FACT complex subunit SSRP1	13.64
DNA replication licensing factor MCM5	7.37
DNA replication licensing factor MCM7	7.47
DNA replication licensing factor MCM3	3.67
DNA replication licensing factor MCM4	6.25
Chromosomal protein D1	0.89
GAPDH1	0.76

S2 cell IP with Gcna		
	Spectral Counts	
Protein	Control	Gcna
Histone H2B	0	4
SSRP1	0	6
DNA topoisomerase 2	0	27
DNA replication licensing factor MCM3	0	14
DNA replication licensing factor MCM5	0	6
DNA replication licensing factor MCM7	0	4
DNA replication licensing factor MCM4	0	2

Figure 3.9. *GCNA* mutants exhibit increased DPC levels. (**A**) Schematic illustrating principle of the RADAR assay. (**B**) RADAR was performed on *Drosophila* ovaries and embryos. Samples were normalized to dsDNA, separated by SDS-PAGE, and silver stained. Red arrows mark examples of differentially enhanced bands in the *Gcna* mutant samples. * marks benzonase added to the prep. (**C**) Proteins enriched in DPCs from $Gcna^{KO}$ *Drosophila* embryos were analyzed by mass spectrometry and presented as enriched over wild-type controls. (**D**) List of proteins that co-immunoprecipate with Gcna expressed in *Drosophila* S2 cells. (**E, F**) Top2 is mislocalized in *Gcna* mutant flies and worms. (**E**) Early *Drosophila* embryos derived from control and $Gcna^{KO}$ females stained for DNA (blue), Top2 (green) and Tubulin (Tub, red). Grayscale shows Top2 alone. Scale bar represents 5 µm. (**F**) Control (N2) and *gcna-1* mutant *C. elegans* gonads stained for DNA (green), TOP-2 (magenta), and staining control XND-1 (yellow). Scale bar represents 20 µm. In collaboration with the Yanowitz lab.

A

	Ovaries		Emb	
Protein	**WT**	**KO**	**WT**	**KO**
Histone H2B	–	–	–	+
SSRP1	–	–	–	+
DNA topoisomerase 2	–	–	–	+
DNA replication licensing factor mcm3	–	–	–	+
Negative elongation factor B	–	+	–	–
rRNA 2'-O-methyltransferase fibrillarin	–	+	–	+
40S ribosomal protein S14b	–	+	–	+
Ubiquitin-40S ribosomal protein S27a	+	+	+	+
Vitellogenin-1	+	+	+	+
Laminin subunit gamma-1	+	+	+	+

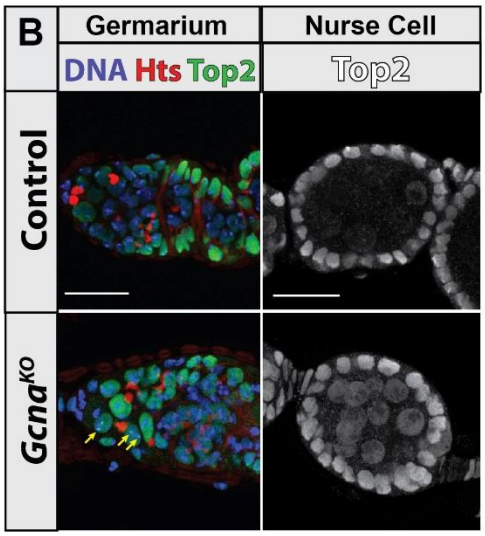

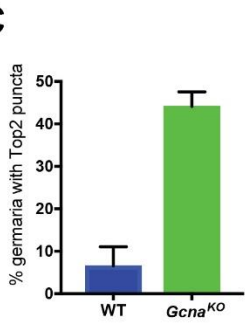

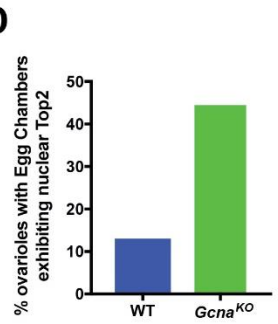

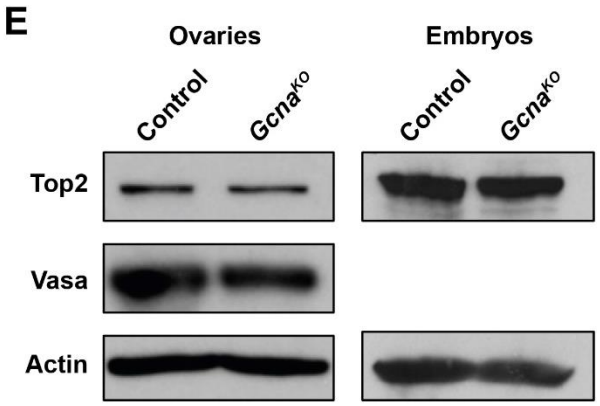

Figure 3.10. *GCNA* mutants exhibit increased DPC levels. (**A**) Summary of DPC mass spectrometry data from control and *Gcna* mutant ovaries and embryos. (**B**) Control and *Gcna*^{KO} mutant ovaries stained for DNA (blue), Hts (red), and Top2 (green). Yellow arrows point to Top2 foci. Scale bars represent 20 µm. (**C**) Quantification of germaria that contain germ cell nuclei with Top2 punctae. (**D**) Percent of ovarioles that contain egg chambers with clear germ cell nuclear Top2 localization. **(E**) Top2 expression levels are not altered by loss of *Gcna*. Western blots of control and *Gcna* mutant extracts probed for Top2 and Vasa and/or actin, as indicated.

Characterization of Drosophila and C. elegans GCNA domain function

The accumulation of DPCs in *Gcna* mutants led us to explore the functional contribution of the conserved metallopeptidase zinc-binding SprT domain and IDR to GCNA function. To this end, we made lines that carried a series of *Drosophila* transgenes or tagged endogenous loci (Figure 3.11A, 3.10A, B). The Gcna-GFP transgene localized predominantly in cytoplasmic punctae, although discrete nuclear punctae could also be detected. Some foci appeared enriched around the nuclear envelope but were distinct from the nuage. During mitosis, Gcna-GFP is associated with dividing chromosomes, in addition to its cytoplasmic localization (Figure 3.11B). The endogenously HA-tagged Gcna protein also exhibited predominantly cytoplasmic localization and association with mitotic chromosomes in ovaries and early embryos (Figure 3.12).

To test the functionality of the SprT domain in *Drosophila* Gcna, we inserted two different UAS-driven HA-tagged transgenes into the same genomic locus: wild-type Gcna and a HE>AA mutant that altered key residues needed for enzymatic activity, based on the characterization of Spartan proteins (Figure 3.11C) (Morocz et al., 2017). These transgenes showed similar cytoplasmic and weak nuclear punctae as described above. When expressed in a *Gcna* mutant background using a *nanos-gal4* driver, the HE>AA protein localized to slightly larger cytoplasmic punctae and was more broadly expressed in late stage nurse cells than wild type protein (Figure 3.11D). Western blot analysis showed that the HE>AA protein was expressed a slightly higher levels than the wild-type transgene (Figure 3.12C). Together, these

experiments suggest that the SprT domain may regulate the size and number of Gcna-labeled condensates and/or overall Gcna protein levels.

Next, we tested the functionality of the *Drosophila* HA-tagged transgenes. The full-length *Gcna* transgene suppressed the excessive formation of both Spo11-dependent and independent breaks that we observed in $Gcna^{KO}$ mutant germ cells (Figure 3.11E, F). As expected, the HE>AA transgene did not rescue these phenotypes to any appreciable degree. However, the HE>AA transgene partially rescued the maternal-effect semi-lethality of embryos derived from *Gcna* mutant females (Figure 3.11G). For both transgenes, rescue of the maternal-effect semi-lethality was accompanied by a decrease in chromosome bridges and other mitotic defects based on DAPI labeling. Thus, the HE>AA transgene demonstrates a partial separation-of-function, revealing a requirement for the SprT domain for DNA damage prevention in the fly germ line, while the IDR domain promotes chromosomal stability during early embryogenesis.

We tagged the endogenous *C. elegans gcna-1* locus at the 5' end with either OLLAS (OmpF Linker and mouse Langerin fusion Sequence) or HA tags. The majority of OLLAS::GCNA-1 and HA::GCNA-1 proteins localized to the cytoplasm under steady-state conditions (Figure 3.11H; S7D). GCNA-1 proteins are maternally-inherited and are ultimately enriched in the primordial germ cell precursors, Z2 and Z3 (Figure 3.12E) which are readily identified by their size and position. In adult germ cells, chromosome squashes allowed us to see small puncta associated with chromosomes in the nucleus (Figure 3.11H; 3.12F), similar to what we observe in *Drosophila.*

We also made a mutant allele, *gcna-1(ea76)* which truncates the C-terminus (of the wild-type protein to retain just the IDR region (Figure 3.11I). While the most robust phenotype observed with the null allele, *gcna-1(ea43)*, was reduced fecundity that began at the F3 generation and became more severe in later generations (Figure 3.4D; 3.11J), *gcna-1(ea76)* had brood sizes greater than or equal to wild type in the F3 and F8 generations. This increase in brood size continued for >15 generations although a subset of the population started to exhibit phenotypes associated with *gcna-1* loss, including a HIM phenotype and sterility. Thus, while loss of catalytic function ameliorates the brood size decline seen in *gcna-1* null mutant animals, the catalytic domain and C-terminus of the protein are required to prevent genome instability across generations. Together with the fly experiments, these data indicate that GCNA is a multi-functional protein with the IDR and SprT domain governing distinct aspects of genome integrity.

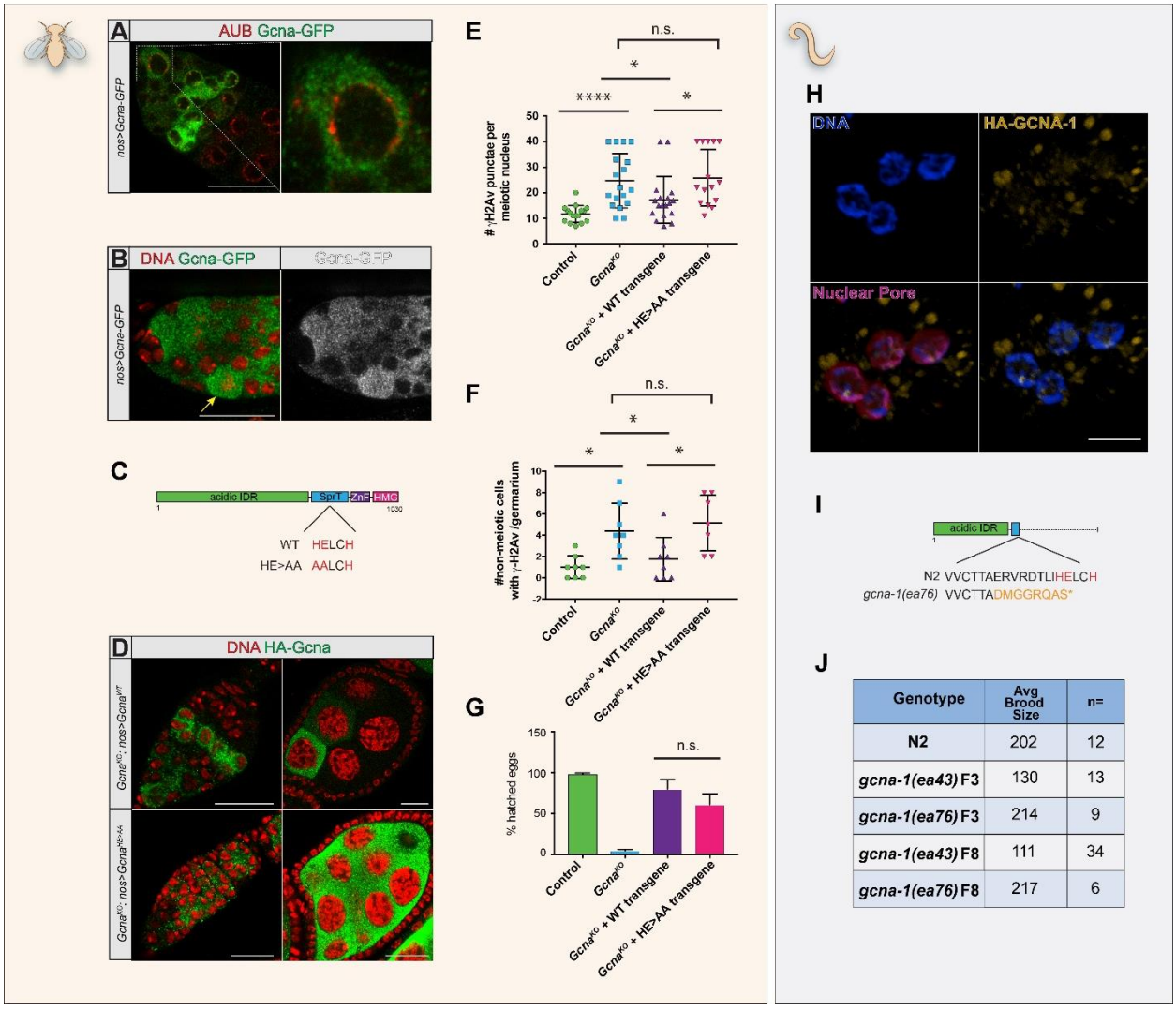

Genotype	Avg Brood Size	n=
N2	202	12
gcna-1(ea43) F3	130	13
gcna-1(ea76) F3	214	9
gcna-1(ea43) F8	111	34
gcna-1(ea76) F8	217	6

Figure 3.11. Functional analysis of GCNA domain structure. (**A, B**) Expression of a *UAS-Gcna*^{WT} transgene tagged at the C-terminus driven by *nanos* (*nos*)-*gal4* shows prominent cytoplasmic staining. Germaria co-labeled for the Gcna-GFP transgene and (**A**) the nuage component, Aubergine (Red) or (**B**) DAPI (red) to visualize DNA. Yellow arrow points to a mitotic germ cell. Scale bars represent 20 µm. (**C**) Structure of the *Drosophila Gcna*^{WT} and catalytic dead, *Gcna*$^{HE>AA}$, mutant transgenes. (**D**) Comparison the Gcna^{WT} and Gcna$^{HE>AA}$ proteins tagged at their N-termini. Note the abundant Gcna$^{HE>AA}$ punctae in the germarium and germ cells. DNA (red), Gcna (anti-HA, green). Scale bars represent 20 µm. (**E-G**) The catalytic dead transgene confers a separation-of-function phenotype and (**E, F**) cannot suppress the accumulation of γH2Av foci in (**E**) meiotic and (**F**) non-meiotic nuclei from wild-type, *Gcna*^{KO}, *Gcna*^{KO}; *nos>Gcna*^{WT}, and *Gcna*^{KO}; *nos>Gcna*$^{HE>AA}$ ovaries, but (**G**) can partially rescue the maternal-effect lethality conferred by loss of *Gcna*. Plotted are the percentage of eggs derived from females of the indicated genotypes that hatch into larvae. (**H**) Expression of *C. elegans* OLLAS::GCNA-1. Germ cells are labeled for DNA (blue), GCNA-1 (anti-OLLAS, yellow), and the nuclear pore antibody mAb414 (magenta). Scale bar represents 5 µm. (**I**) Structure of the *C. elegans* "IDR-only", C-terminal truncation allele, *gcna-1(ea76)*. (**J**) Comparison of brood sizes from N2 control, and homozygous, F3 and F8 *gcna-1(ea43)* null and *gcna-1(ea76)* truncation mutants. The IDR-only mutation does not exhibit the rapid transgenerational sterility seen in the null. In collaboration with the Yanowitz lab.

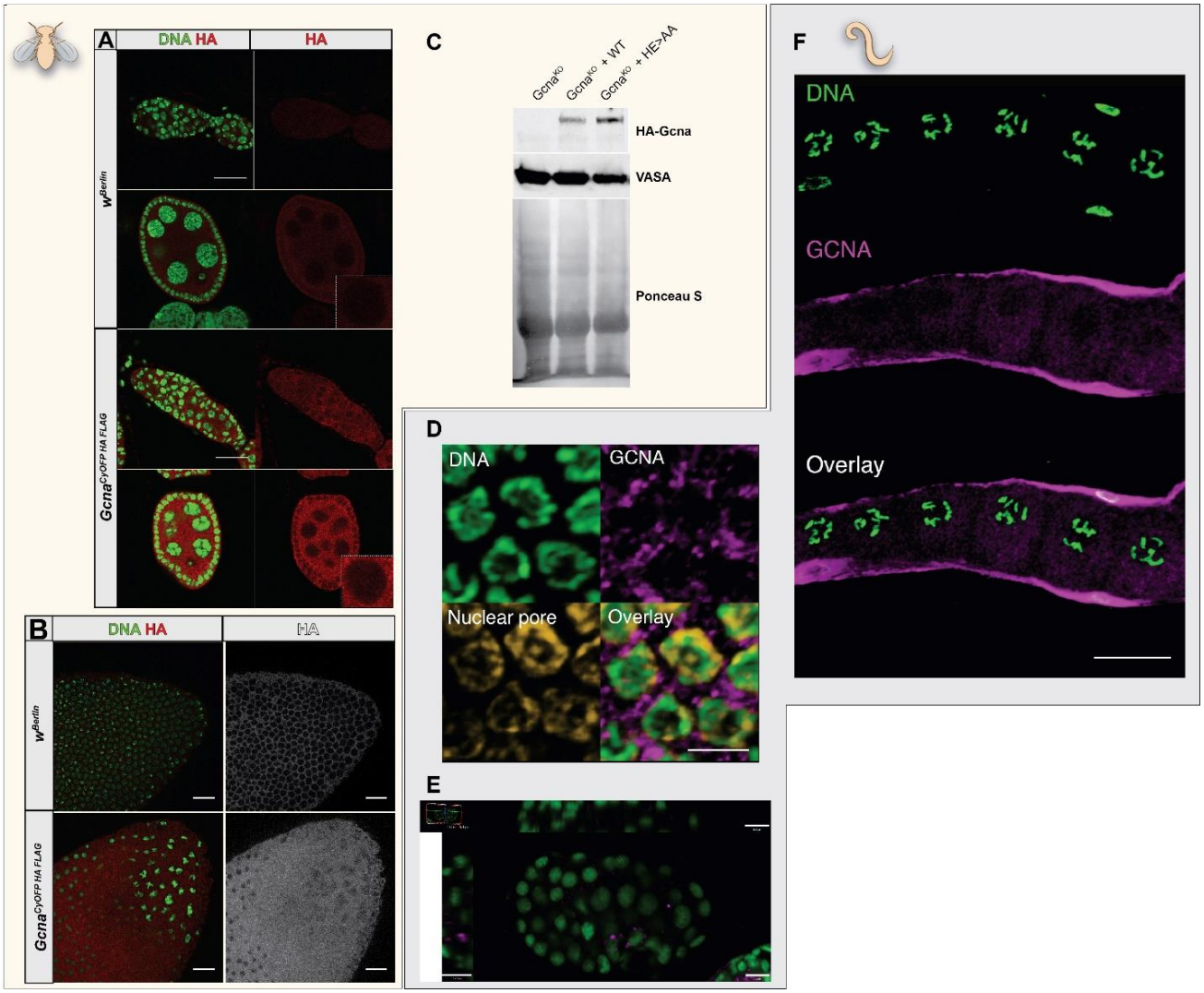

Figure 3.12. Functional analysis of GCNA domain structure. (**A**) Control w^{Berlin} and $Gcna^{CyOFP\ HA\ FLAG}$ ovaries stained for HA (red) and DNA (green). (**B**) Control w^{Berlin} and $Gcna^{CyOFP\ HA\ FLAG}$ embryos stained for HA (red) and DNA (green). (**C**) Western blot showing expression of indicated *Gcna* transgenes in the $Gcna^{KO}$ background. (**D**) Germline squashes of HA::GCNA-1 animals stained with DNA (DAPI, green), GCNA-1 (anti-HA, magenta), and nuclear pores (mAb414, yellow). Faint nucleoplasmic staining of GCNA-1 can be observed. (**E**) Primordial germ cell expression of GCNA-1 is seen in OLLAS::GCNA-1 embryos stained for DNA (green) and GCNA-1 (anti-OLLAS, magenta). Shown are single plane image from a Z-stack. Scale 5 µm. (**F**) OLLAS::GCNA-1 germ lines were stained for DNA (green) and GCNA-1 (anti-OLLAS, magenta). Granular cytoplasmic staining is readily observed in the diplotene nuclei. Scale 20 µm. In collaboration with the Yanowitz lab.

Conservation of GCNA function in zebrafish

To characterize *Gcna* function in a vertebrate, we generated *gcna* mutant alleles in zebrafish including a 7 bp deletion (*mut1*) and a complex insertion of 9 bp and 11 bp (*mut2*) both of which lead to early frameshifts, predicted to result in severely truncated proteins in collaboration with the Amatruda lab (Figure 3.13A,B). The progeny of *gcna* mutant females displayed widespread morphological defects and cell death (100% penetrant; n>100 embryos) (Figure 3.13C,D). Close examination of these early embryos revealed asynchronous mitotic divisions and tangled chromosomes, in contrast to wild-type controls (Figure 3.13E). These results indicate that disruption of zebrafish *gcna* results in maternal-effect lethality marked by chromosome instability remarkably similar to the phenotypes observed in flies and worms. To test whether *gcna* loss also resulted in elevated DPC levels across species, we performed RADAR on zebrafish embryos. This analysis showed that disruption of *gcna* resulted in modestly increased levels of DPCs (Figure 3.13F).

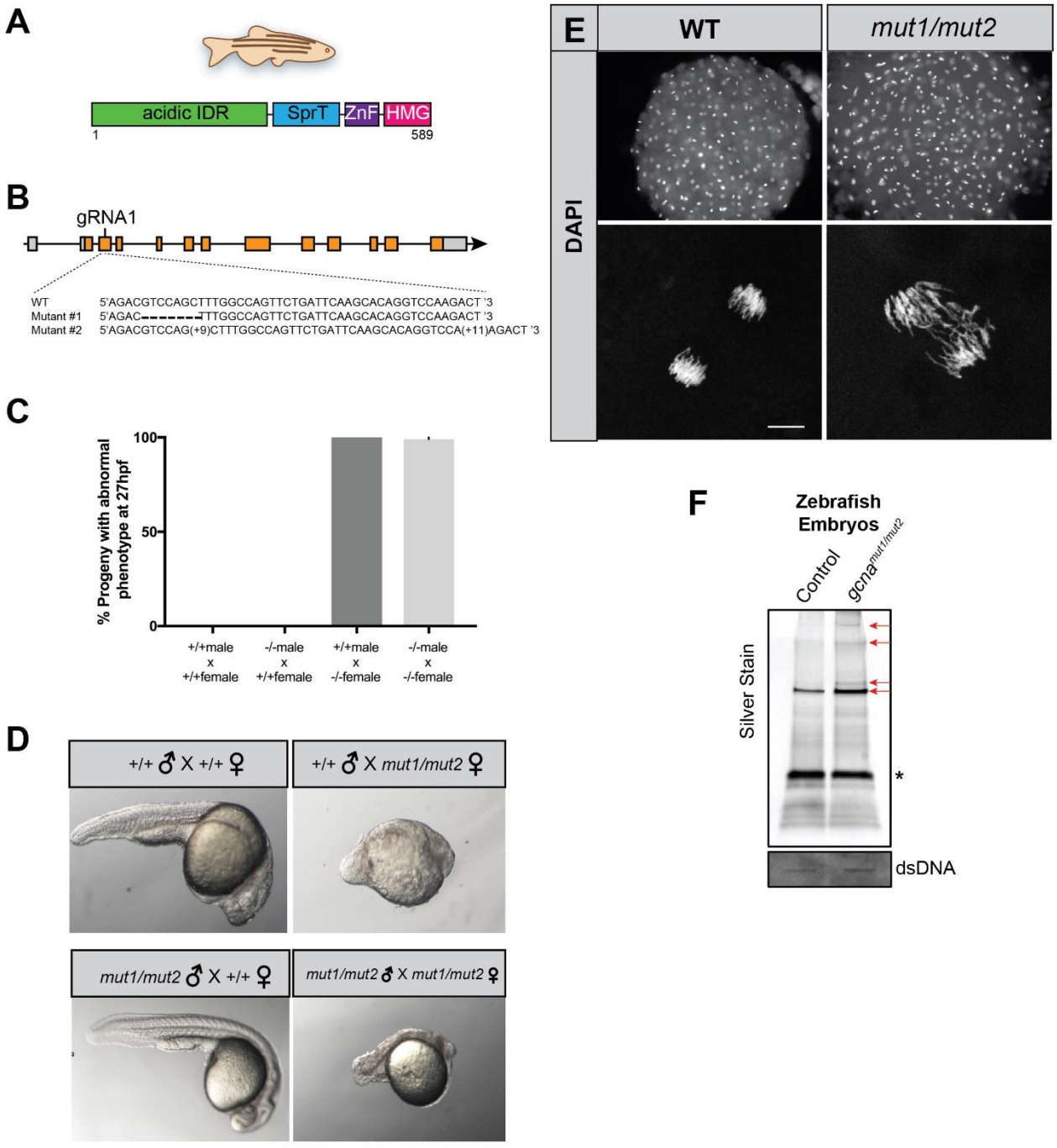

Figure 3.13. GCNA function is conserved in vertebrates. (**A**) Domain structure of the zebrafish GCNA protein. (**B**) Organization of the zebrafish *gcna* gene showing the lesions in the *mut1* and *mut2* alleles. (**C, D**) Zebrafish embryos derived from mutant *gcna* mutant females exhibit profound maternal-effect defects, regardless of the paternal genotype. (**C**) Quantification of defects and (**D**) Representative embryos from indicated crosses. (**E**) Fixed, DAPI-stained embryos derived from mutant *gcna* mutant females exhibit asynchronous divisions and extensive chromosome bridges during early development. Scale bar represents 10 µm. (**F**) RADAR was performed on zebrafish embryos, as described in Figure 4A, B. Samples were normalized to dsDNA input, separated by SDS-PAGE, and silver stained. Red arrows mark bands increased in *gcna* mutants. * marks benzonase. In collaboration with the Amatruda lab.

Loss of GCNA correlates with genomic instability in human germ cell tumors

Our work in flies, worms, and zebrafish indicates that GCNA regulates genome stability across species. Whereas in humans, germ cells are largely inaccessible, germ cell tumors provide a window into the genes that control genome integrity. In collaboration with the Amatruda lab, we therefore performed whole-exome and targeted deep sequencing, SNP array, DNA methylation array, and RNA sequencing on a cohort of 233 patients with pediatric germ cell tumors (GCTs), and conducted an integrated analysis of the data analyzed (Xu and Amatruda, in preparation). To investigate tumor suppressor genes that are frequently silenced by copy number (CN) loss (based on SNP array data) and promoter hypermethylation (base on DNA methylation array data) in GCTs, we examined 94 of 233 GCTs in our cohort that were processed by both array technologies. In these 94 GCTs, we calculated the percentage with either CN loss, promoter hypermethylation, or both, for *GCNA* and 441 known cancer genes (from Catalogue of Somatic Mutations in Cancer (COSMIC) database). Interestingly, we found *GCNA* has the highest alteration frequency (66%, 62 out of 94 cases) among all 442 genes studied here (Figure 3.14A,B), suggesting *GCNA* to be a top candidate for a tumor suppressor involved in GCT development. No somatic protein-altering mutation was found in *GCNA* gene through whole-exome and targeted deep sequencing analysis in 137 GCT cases.

As expected, CN loss and/or promoter hypermethylation in *GCNA* was correlated with significantly lower *GCNA* expression in tumors, compared to GCTs without alterations (Figure 7C). Thus, it appears that genetic and epigenetic alterations are responsible for down-regulation of *GCNA* expression in human GCTs. Notably, we observed a significant association between low *GCNA* expression and poor GCT patient survival (Figure 3.14D,

hazard ratio = 0.66, 95% CI 0.45-0.96, log-rank test, P = 0.032), which suggests that *GCNA* might serve as a potential prognostic marker.

To further investigate whether genetic and epigenetic alterations in *GCNA* gene are associated with genome instability, we studied the frequency of copy number amplification and loss on a genome-wide scale. We found that tumors with alterations in *GCNA* gene display significantly elevated frequency of both copy number amplification and loss events (Figure 3.14E), supporting the idea that loss of *GCNA* expression may contribute to human germ cell tumorigenesis by promoting genome instability.

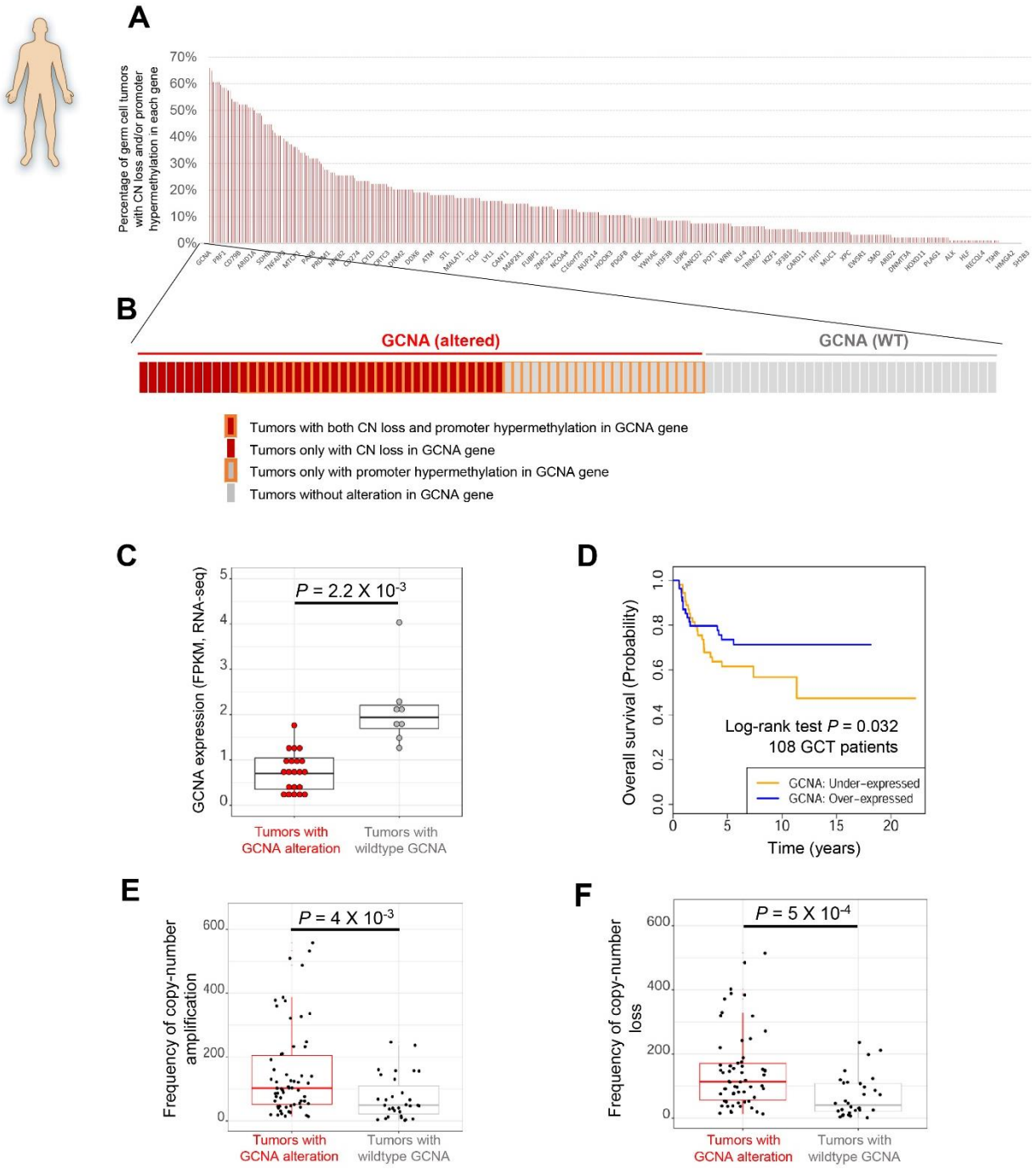

Figure 3.14. *GCNA* is frequently altered in pediatric germ cell tumors (GCTs) and is associated with poor patient survival and genomic instability. (**A**) *GCNA* genes display the most frequent copy-number loss and promoter hypermethylation in 94 childhood patients with GCTs. (**B**) Frequency of copy-number loss and promoter hypermethylation of *GCNA* gene in pediatric GCTs. (**C**) Low GCNA expression in pediatric GCTs is found in tumors with alterations of the *GCNA* locus. (**D**) Low GCNA expression is significantly associated with poor survival of GCT patients. (**E,F)** GCTs with copy number loss of *GCNA* exhibit elevated frequencies of both copy number (**E**) amplification and (**F**) loss relative to tumors with normal *GCNA* copy number. In collaboration with the Amatruda lab.

Discussion

Here, we report the initial functional characterization of GCNA as a key regulator of genome stability within germ cells and early embryos and as a putative tumor suppressor in GCTs. *Gcna* mutants exhibit remarkably similar phenotypes in flies, worms, and zebrafish indicating that GCNA carries out conserved functions throughout the animal kingdom. Germ cells must contend with many distinct challenges imposed by their unique biology and the dangers of various endogenous and exogenous genotoxic threats. Loss of GCNA compromises the ability of germ cells to handle these stresses and disrupts a number of seemingly disparate processes including germ cell development and maintenance, chromosome segregation, the cell cycle, DNA replication, and the formation of programmed DSBs during meiosis. Our findings suggest that these processes may be linked together through GCNA in unexpected ways. Given its enriched germline expression and critical function, GCNA should be considered, alongside with Nanos, Vasa, and Piwi as an essential player in germ cell biology.

How can GCNA influence so many different processes within germ cells? Our data indicate that the phenotypes exhibited by *Gcna* mutants do not extend from one specific malfunction, but rather from disruption of several distinct functions. Our genetic experiments in flies and worms indicates specific functions of GCNA can be attributed to distinct domains (Figure 3.11). For example, SprT enzymatic activity appears necessary for the prevention of excessive Spo11-dependent and -independent DNA damage during *Drosophila* oogenesis. By contrast, the SprT mutant transgene partially rescues the maternal-effect semi-lethality of *Gcna*

mutants, indicating this enzymatic activity is not essential for the proper regulation of chromosome segregation and cell cycle during early embryogenesis. Similarly, in *C. elegans*, *gcna-1* alleles which encode just the amino-terminal IDR domain do not exhibit a reduction in average brood size over the first eight generations. This contrasts with the loss of fecundity conferred by the null allele, again indicating that many germ cell activities depend on the IDR. This separation of structure and function provides an important framework for further understanding how GCNA ensures genomic stability across species. Of note, the mouse protein is comprised of just an IDR domain (Carmell et al., 2016), raising the possibility that the chromosome segregation and cell cycle functions may represent the core activities of these proteins.

Given the modest increase of DPCs within *Gcna* mutants (Figure 3.9) and the failure of the HE>AA mutant transgene to rescue Spo11-dependent and -independent damage in *Drosophila* ovaries (Figure 3.11), it is tempting to speculate that the SprT domain of GCNA serves the same function as it does in Spartan, namely to regulate DPCs that form on chromosomes (Stingele et al., 2017). Indeed, a recent study found that human GCNA/ACRC is recruited to DPCs in a SUMO-dependent manner (Borgermann et al., 2019). Consistent with these results, we find GCNA associates with replication machinery, based on its ability to immunoprecipitate components of the MCM complex (Figure 3.9) and *Gcna* mutants likely suffer from replicative stress based on increased RPA foci in *Drosophila* cells (Figure 3.8), microsatellite instability in worms (Figure 3.8), and copy number amplification and loss in human germ cell tumors (Figure 3.14). This raises the question regarding the separate requirements for GCNA and Spartan. Germ cells may have an increased DPC load compared

to somatic cells, and therefore require alternative mechanisms for dealing with these lesions. For example, germ cells undergo extensive epigenetic reprogramming. These reactions, such as histone demethylation, produce cross-linking agents as by-products (Stingele et al., 2017). In addition, germ cells encounter enzymatic DPCs during meiotic DSB induction when Spo11 acts through a topoisomerase-like mechanism and becomes covalently attached to DNA at the break site (Keeney et al., 1997) While the MRN complex clears these adducts through endonuclease cleavage (Neale et al., 2005) perhaps GCNA represents an alternative mechanism for clearing Spo11 off of meiotic chromosomes in order to ensure that all lesions are repaired prior to embryogenesis. Given the increase of Spo11-induced breaks in flies, where very few meiotic breaks are made, GCNA may have evolved to limit either Spo11 activity or the amount of Spo11 that reaches the DNA, perhaps through sequestration of Spo11 or its accessory factors in the cytoplasm. The dramatic accumulation of Top2 in a subset of nuclei in *gcna-1* mutant worms and on mitotic DNA in mutant flies is also consistent with a sequestration model. Lastly, germ cells, particularly oocytes, experience extensive periods of cell cycle arrest during which they may accumulate DPCs that would otherwise interfere with chromatin-based processes upon fertilization. Perhaps GCNA also provides a replication-independent means for clearing or preventing such lesions.

IDR proteins have emerged as important regulators of germ cell biology. Many proteins that play essential roles in germ cells, such as Vasa, Oskar, Bucky ball and MEG-3, contain IDRs. These IDRs often control the ability of these proteins to undergo phase transitions, allowing for the compartmentalization of various RNAs and proteins (Krishnakumar and Dosch, 2018). We are just beginning to understand the functional significance of this molecular

behavior. The IDR of GCNA is essential for its function within germ cells. While the primary amino acid sequence of GCNA's IDR has diverged, this region has continued to retain a high percentage of aspartic acid and glutamic acid residues. The importance of this distinct composition remains unknown, but perhaps it regulates the stability of GCNA or its ability to form condensates. Our expression studies indicate that GCNA localizes in a discrete cytoplasmic punctae in interphase and on chromosomes during mitosis. In flies and worms, the GCNA IDR promotes proper chromosome segregation and cell cycle regulation. Perhaps GCNA undergoes phase transitions and thereby controls the availability, assembly, or function of factors needed for these processes.

In flies and zebrafish, loss of *Gcna* leads to profound maternal-effect phenotypes, marked by chromosome segregation defects, chromosome bridges, and cell cycle asynchrony. Worm *gcna-1* mutants also exhibit chromosome bridges and X-chromosome loss, albeit at a lower frequency or only in later generations. The chromosome bridges that form in $Gcna^{KO}$ fly embryos often contain the heterochromatic 359-Bp repeats found on the X chromosome. This satellite sequence is responsible for the chromatid separation defects that occur in hybrid progeny of *D. melanogaster* and *D. simulans* (Ferree and Barbash, 2009). In addition, recent work has shown that loss of *mh*, which encodes the *Drosophila* homolog of Spartan, also results in chromosome bridges that contain 359-bp sequences (Tang et al., 2017). While, our genetic experiments indicate that GCNA and Spartan proteins act in parallel pathways, they may converge on a mechanism that helps to resolve segregation defects involving heterochromatic sequences. Interestingly, we observe the formation of micronuclei and chromosome fragmentation in *Drosophila* and *C. elegans Gcna* mutants. Similar events are

thought to presage chromothripsis in cancer cells (Stephens et al., 2011) Sequencing data in the accompanying paper indicate that *C. elegans Gcna* mutants display molecular signatures consistent with chromothripsis (Davis et al. (2019)). Thus, the further study of GCNA may provide a model for understanding the origins of this newly recognized process and for determining how germ cells protect themselves from widespread chromosome re-arrangements in the face of DNA damage.

Underscoring the importance of GCNA in cancer, we have found that *GCNA* is among the most highly mutated genes in pediatric germ cell tumors and its loss is associated with pathogenicity. The platinum-resistance of certain GCTs (Batool et al., 2019) necessitates the discovery of novel druggable targets, and our studies suggest GCNA may be such a therapeutic target. The association of GCNA with both gene amplification and loss in GCT samples suggests that tight regulation of GCNA may be critical. Future studies on gain and loss of GCNA function will help elucidate its role as a driver of tumorigenesis.

Germ cells have many unique features in regard to reprogramming, regulation of the cell cycle and DNA repair. The study of *GCNA* will provide further insights into how these processes are coordinated with each other to ensure the faithful transmission of genetic material from one generation to the next. In addition to the observed correlation between loss of *GCNA* and human germ cell tumors, we anticipate *GCNA* function likely influences other aspects of human fertility and transgenerational inheritance across sexually reproducing species.

CHAPTER FOUR
Maternal GCNA is necessary for proper spindles in the syncytial embryo

Introduction

Life depends on successful cell division. A human zygote must accurately divide ~3.72 X 10^{13} times to form an adult (Bianconi et al., 2013). A cell must duplicate its genome and package it equally into two daughter cells to successfully proliferate. The cell accomplishes this feat with a bipolar, fusiform spindle which helps to separate half of the chromosomes into each new cell.

The mitotic spindle ensures the faithful transmission of chromosomes to the daughter cells. The spindle is comprised of dynamic microtubules and approximately 1,000 microtubule associated proteins including motors, crosslinkers, microtubule polymerases and microtubule depolymerases (Sauer et al., 2005). There are three major types of microtubules in the mitotic spindle: kinetochore microtubules, interpolar microtubules, and astral microtubules. The bundle of kinetochore microtubules (K-fiber) anchor the spindle poles to the chromosome by attaching to the kinetochore. Interpolar microtubules (ipMT) comprise the central spindle emanating from opposite poles with their plus ends overlapping in the spindle midzone. Crosslinkers often reside in this overlapping region. In *Drosophila,* the plus end directed motor, kinesin-5, is present along the cross-bridges between adjacent microtubules, which provides midzone pushing during spindle expansion (Sharp et al., 1999). The astral

microtubules (aMT) extend outwards from the centrosomes and contact the cell cortex. The centrosome is the microtubule organizing center (MTOC), which in most cases is comprised of a pair of centrioles surrounded by the pericentriolar matrix (PCM). However, plants and oocytes undergo acentriolar spindle assembly.

In a newly fertilized zygote, the sperm contributes two centrioles and the embryo is maternally loaded with the components of the PCM. Centrosome duplication is tightly regulated because supernumerary centrosomes can affect spindle morphology and chromosome attachment compromising the fidelity of chromosome segregation. SAK/Plk4 controls centriole duplication (Bettencourt-Dias et al., 2005). In *Drosophila,* Asterless (Asl), a Cep152 ortholog, recruits Plk4 to the centriole. Interestingly, Asl is able to both activate and inhibit Plk4's kinase activity depending on its own phosphorylation status (Boese et al., 2018). Polo is important for centrosome maturation by phosphorylating centrosomin (Cnn) which drives its scaffolding assembly (Conduit et al., 2014; Eisman et al., 2015). Polo also recruits γ-TuRC to the centrosome (Donaldson et al., 2001). Cnn is important for recruiting γ-tubulin to the centrosome and plays an important role in centrosome maturation and nucleating microtubules (Conduit et al., 2014; Zhang and Megraw, 2007).

The *Drosophila* embryo undergoes 13 rounds of rapid, synchronous cell division in a syncytium with a modified cell cycle that alternates between S- and M- phases. During cycle 14 the embryo cellularizes. In the early embryo the centrosome controls the dynamics of the cell cycle (Blake-Hedges and Megraw, 2019).

Results

The mitotic spindle must rapidly and robustly assemble microtubules to properly segregate sister chromatids. Microtubules are nucleated to form the spindle from six different complexes: centrosomes, kinetochores, chromosomes, via RanGTP, via the chromosomal passenger complex (CPC), and microtubule dependent microtubule nucleation (Petry, 2016). These complexes work together to ensure proper spindle assembly and maintenance.

Loss of maternal *GCNA* disrupts spindle microtubules. The spindles in embryos from *GCNA* mutant mothers have ipMT and K-fibers present, but they have a lower density of microtubules throughout the spindles compared to embryos from wildtype mothers (Figure 4.1). This decreased density of microtubules could indicate a defect in microtubule dependent microtubule nucleation. Microtubule dependent microtubule nucleation exponentially increases microtubules while preserving the polarity of the fibers because new fibers branch from pre-existing fibers. This type of nucleation is dependent on γ-tubulin ring complex (γ-TuRC) and augmin (Goshima et al., 2008; Uehara et al., 2009).

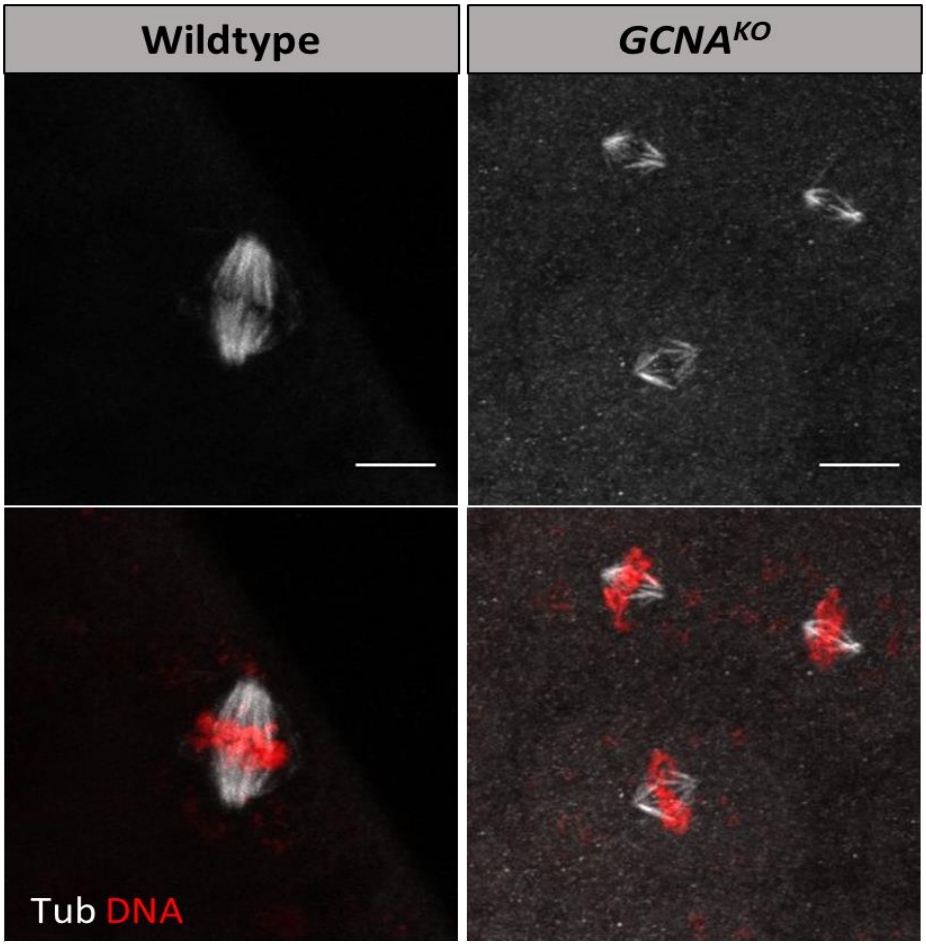

Figure 4.1. Loss of maternal *Gcna* disrupts spindle microtubules. 0-2 hour embryos from wildtype and *Gcna*^{KO} mothers stained with α tubulin (white) and DAPI (Red). The spindles from *Gcna*^{KO} mothers have a lower density of microtubules. Scale bar represents 10 μm.

Embryos lacking maternal *GCNA* have multipolar spindles (Figure 4.2). Spindles in embryos from wildtype mothers have two poles and thus are referred to as a bipolar spindle. Bipolar spindles favor amphitelic attachments of microtubules to kinetochores in which sister kinetochores are attached to microtubules from opposing poles. Multipolar spindles favor merotelic attachments of microtubules to kinetochores wherein the kinetochore of a sister chromatid is attached to microtubules emanating from two different poles. Merotelic

attachments cause problems during anaphase which leads to lagging chromosomes and contributes to genomic instability (Gregan et al., 2011).

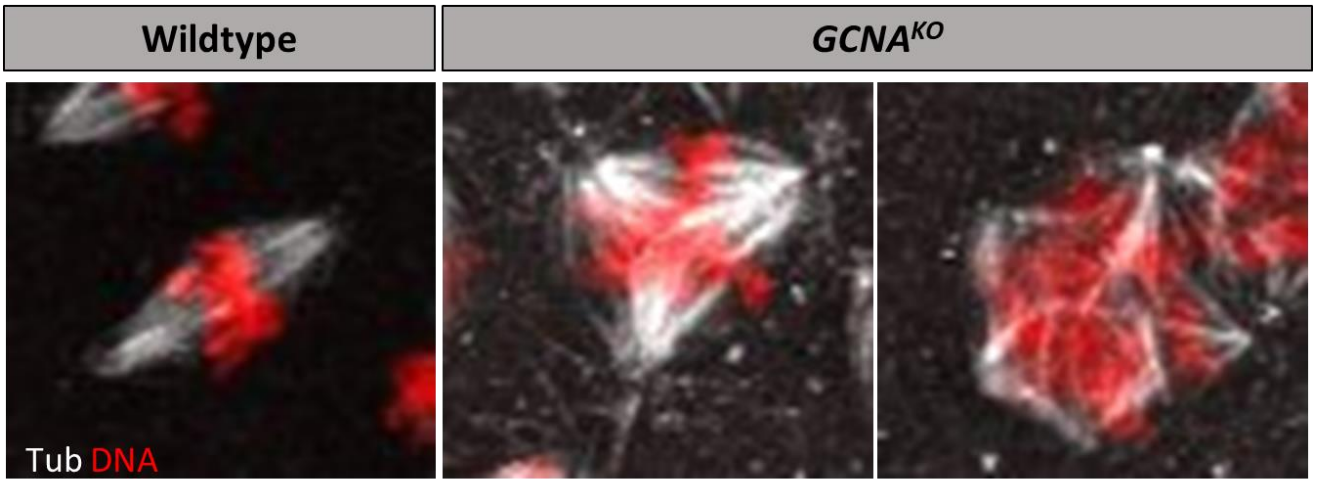

Figure 4.2. Spindles from *Gcna*^{KO} mothers are multipolar. 0-2 hour embryos from wildtype and *Gcna*^{KO} mothers stained with α tubulin (white) and DAPI (Red). The spindles from *Gcna*^{KO} mothers have multiple poles instead of the normal two poles as seen in wildtype.

The current view in the field is that a major contributor to multipolar spindles is supernumerary centrosomes. Thus, I looked at centrosome numbers in the embryo. Loss of maternal *GCNA* disrupts centrosome number. In embryos from *GCNA* mutant mothers, more than two centrosomes per nucleus are often observed (Figure 4.3). Furthermore, some spindle poles in multipolar spindles lack centrosomes as seen by the absence of Asl staining at the pole (Figure 4.3B).

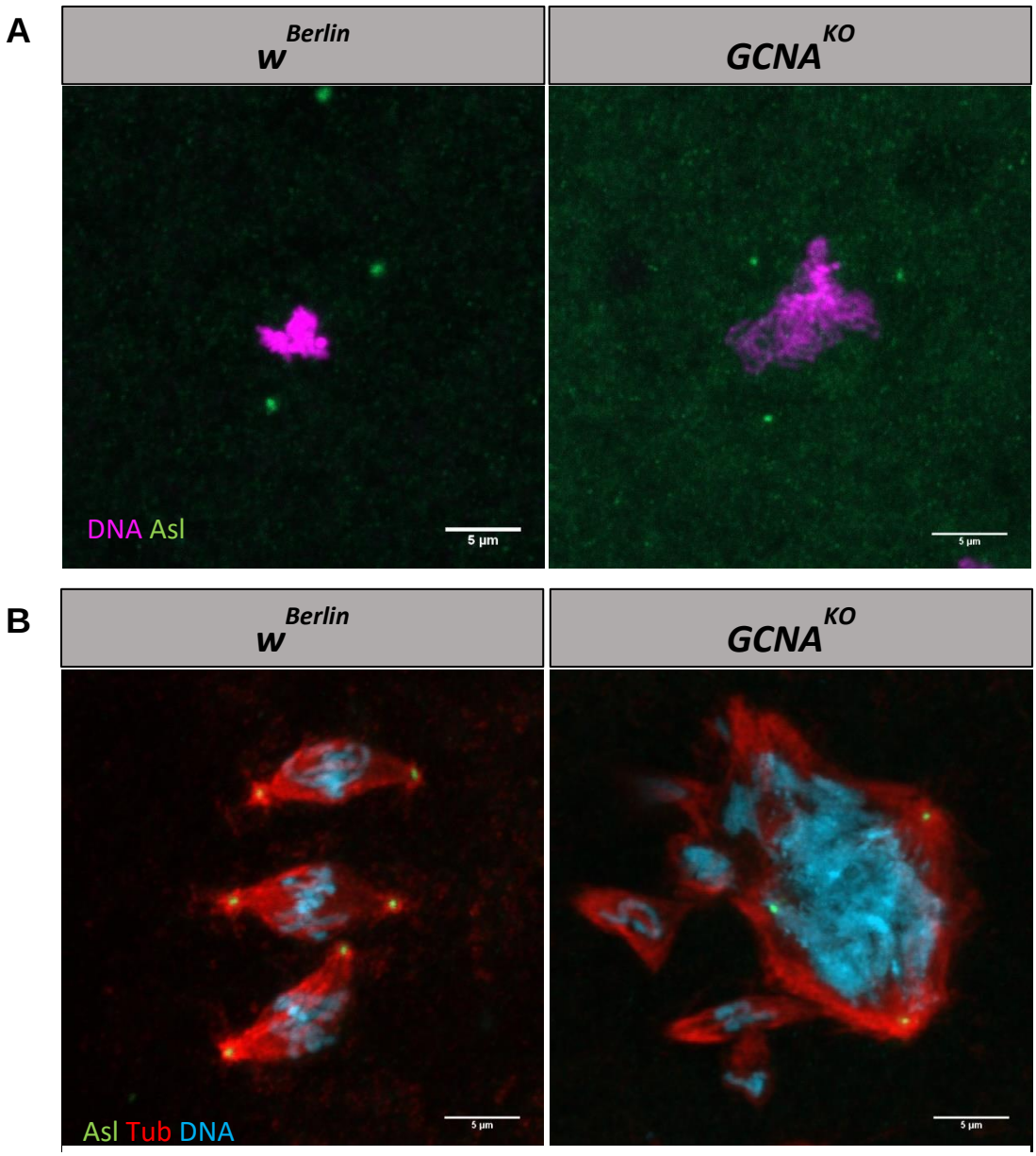

Figure 4.3. Loss of maternal *Gcna* disrupts centrosome number. (**A**) 0-2 hour embryos from wildtype and *Gcna*^{KO} mothers stained with Asl (green) and DAPI (magenta). Scale bar represents 5 µm. (**B**) 0-2 hour embryos from wildtype and *Gcna*^{KO} mothers stained for Asl (green), α tubulin (red), and DAPI (cyan). Scale bar represents 5 µm.

To gain a deeper understanding of the spindle assembly, I looked at polo localization in the *Drosophila* embryos. Polo is strongly localized to the centrosomes and kinetochores as

well as distributed along the spindle during metaphase and anaphase. Polo is not properly localized in embryos lacking maternal *GCNA.* Polo is very weakly localized to the centrosomes and sparsely distributed along the spindles in embryos from *GCNA* mutant mothers (Figure 4.4). *polo* mutants display a variety of mitotic defects, but these defects primarily occur due to microtubule organizing centers not functioning properly. *polo*^{1} mutant embryos display spindles with broad poles or monopolar spindles (Llamazares et al., 1991). In spermatocytes from *polo*^{1} males the central spindle fails to form thus disrupting cytokinesis (Carmena et al., 1998). Polo recruits γ-TuRC and γ-tubulin to the centrosome and recruits augmin to mitotic spindles (Donaldson et al., 2001; Savoian and Glover, 2014). Further, partially purified centrosomes can nucleate microtubules on a glass slide. When the purified centrosomes are salt stripped with potassium iodide, they lose the ability to nucleate microtubules. Microtubule nucleation can be restored with supernatant extract from wildtype embryos but not *polo*^{1} embryos (do Carmo Avides et al., 2001). Supernatant from *polo*^{1} embryos with added phosphorylated Asp (abnormal spindle) protein can restore microtubule nucleating capability (do Carmo Avides et al., 2001). Thus, the spindle defects observed in embryos lacking maternal *GCNA* may likely be due to insufficient Polo activity.

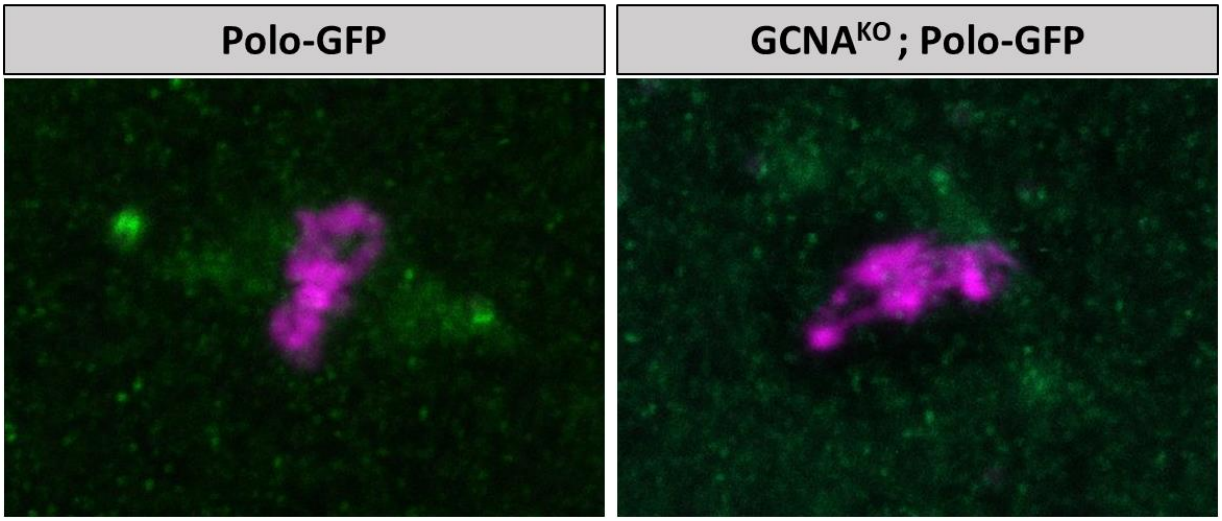

Figure 4.4. Polo is not properly localized to the centrosome upon loss of maternal *Gcna*. 0-2 hour embryos from control (*Polo-GFP*) and *Gcna*^{KO}*; Polo-GFP* mothers stained with GFP (green) and DAPI (magenta).

Discussion

A major question remains as to why GCNA is needed for proper spindle assembly in the early embryo but not in other adult tissues. One possibility is that the early embryo has a high cytoplasmic to chromosome ratio compared to other cells, and thus GCNA helps assemble the spindle when the necessary components are more dilute. The IDR of GCNA could act as a scaffold or phase shift the necessary spindle components. Additionally, many of the checkpoints, such as the spindle assembly checkpoint, are not fully active in the early embryo. Therefore, GCNA could act as a safeguard to early spindle formation when the normal checkpoints are not as active. Another possibility is GCNA is needed to efficiently assemble spindles very rapidly. The *Drosophila* embryo goes from a single zygotic complement to about 5,000 nuclei in roughly 2 hours. The embryo undergoes a modified cell cycle of alternating S-

and M- phases that are approximately 10 minutes. Thus, GCNA may be needed to efficiently assemble the spindle in the modified, rapid cell cycles in the early embryo but not in adult somatic tissues where the cell cycle is longer.

Spindle abnormalities may be a major contributor to genome instability in *GCNA* mutants. Loss of maternal GCNA causes multipolar mitosis which favor merotelic attachments of kinetochores. Merotelically attached kinetochores are particularly deleterious to the cell because they can pass the spindle assembly checkpoint (Gregan et al., 2011). Yet, merotelic attachments often lead to lagging chromosomes and can lead to centromere fission wherein a sister chromatid breaks at or near the centromere. Centromere fission may lead to the formation of a dicentric chromosome in which the chromosome harbors two centromeres. Dicentric chromosomes are inherently unstable because microtubules from opposing poles may attach to each centromere, subsequently causing further rounds of chromatid breakage and fusion. Ultimately this breakage and fusion cycle results in massive and complex genome rearrangement and aneuploidy.

Aneuploidy is often deleterious to the cell and to the organism. Aneuploid cells grown in normal culture conditions proliferate slower than their euploid counterparts, indicating that aneuploidy has a fitness cost (Williams et al., 2008). However, under harsh conditions or rapid change aneuploidy can have a competitive advantage. Under specific microenvironments, such as oxygen deprivation, nutrient stress, or chemotherapeutic stress, aneuploid cells can gain a proliferative advantage. Further, focal amplification of oncogenes or deletions of tumor suppressors can give the cell a proliferative advantage. The Cancer Genome Atlas (TCGA) has shown that nearly all cancers have significant chromosomal aberrations from genomic data

they have gathered on numerous cancer types (Weinstein et al., 2013). High genomic instability correlates with more aggressive tumors and poorer patient prognosis. Thus, genomic instability caused by the loss of *GCNA* may be an early driver of tumorigenesis in GCTs and may also contribute to drug resistance. Genomic instability in cells lacking *GCNA* may be caused by both an increased DPC burden as well as spindle abnormalities.

CHAPTER FIVE
Conclusions and Future Directions

Conclusions

GCNA promotes genome stability and preserves fertility in *C. elegans*, *Drosophila*, zebrafish, and humans. The protease domain of GCNA is important for limiting both meiotic and non-meiotic damage; whereas, the IDR of GCNA is important for ensuring proper chromosome segregation in the early embryo. The spindles in the early embryo from *GCNA* mutant mothers show several defects, including decreased microtubule density and multipolar spindles. Multipolar spindles are a major contributor to genome instability because the genetic content often does not segregate equally into two daughter cells. Thus, multipolar spindles lead to the loss of entire chromosomes. The loss of the X chromosome in *Drosophila* embryos is currently thought to be how gynandromorphs are formed, resulting in diplo/haplo mosaics (XX/XO). However, there is evidence in birds that fertilization of an egg by two sperm can lead to the formation of gynandromorphs (Zhao et al., 2010). Gynandromorphs from *GCNA* mutant mothers are unlikely to be formed by fertilization of two sperm and are likely occur through the loss of the X chromosome. Recessive markers on the paternal X chromosomes would not be visible in the gynandromorphs in the case of fertilization from two sperm and capturing of a polar body.

Future Directions

GCNA mutants have an increase in DPCs (Figure 3.9, Figure 3.13). Further embryos lacking maternal *GCNA* have multipolar spindles (Figure 4.2, Figure 4.3). Thus, GCT that lack GCNA or have reduced GCNA expression should be tested for an increased DPC burden and spindle defects. If the tumors do exhibit these defects, then microtubule drugs or DNA-protein crosslinkers could be explored as a treatment for GCTs lacking *GCNA* expression. Recent studies have shown that while a low amount of chromosome missegregation contributes to tumorigenesis, large amounts of genomic instability and chromosome missegregation suppress tumor growth rates (Silk et al., 2013). Thus, exacerbating the genomic instability in the GCT could suppress the tumor growth and lead to a better prognosis for patients with GCTs that lack GCNA.

In many organisms, the sperm contributes the centriole and the oocyte contributes the PCM components to build the first mitotic spindle (Callaini and Riparbelli, 1996; Sun and Schatten, 2007). The sperm centrioles nucleate astral microtubules, called the sperm aster, guiding the sperm to capture the female pronucleus and complete fertilization. Sperm from *polo*^{1} males fail to form the sperm aster, so the two pronuclei stay separated and undergo a limited number of haploid divisions (Riparbelli et al., 2000). Perhaps infertility in human male patients with mutated GCNA or altered GCNA expression could be due to defects in the sperm centrioles and their ability to nucleate microtubules. Intracytoplasmic Sperm Injection could be used to asses if the centrosomes in the sperm from these patients are functional (Schatten and Sun, 2009).

APPENDIX A
Primers Used

FISH probes
X chromosome 5'-/5Cy3/TTTTCCAAATTTCGGTCATCAAATAATCAT-3'
2nd chromosome 5'-/5Cy5/AACACAACACAACACAACACAACACAACAC-3'
***Drosophila* CRISPR**
CG14814_arm1_F
GCATCACCTGCGCATTCGCTTGTGAGATTGGCTCGTTGG
CG14814_arm1_R
GCATCACCTGCGCATCTACTTTCTGGTCGTTCCTCTTTTCTGG
CG14814_arm2_F
GCATGCTCTTCTTATTAAAGGCGATGCTTGGACTCATT
CG14814_arm2_R
GCATGCTCTTCTGACTGGCTGTACTCGGGAATCTG
CG2694_arm1_F
AAAACACCTGCAAAATCGCTGCTTAACGCTTTCGTAGTACTGC
CG2694_arm1_R
AAAACACCTGCAAAACTACCGCCACTATTGTTCAACTGTGC
CG2694_arm2_F
AAAAGCTCTTCATATCTCCGGCAGGCGCACAGCACAGATCC
CG2694_arm2_R
AAAAGCTCTTCAGACTTCCATTTCTTCAAACATGCG
GCNA gRNA1 5'-CTTCGAGAGGAACGACCAGAAAACA-3'
GCNA gRNA2 5'-CTTCGTCGGCCGGCGGTGTTGGTAA-3'
CG2694 gRNA1 5'- CTTCGTTGAACAATAGTGGCGTAC-3'
CG2694 gRNA2 5'- CTTCGAGCTTGGCTTCGACGCCTC-3'
CG11322 gRNA1 5'-CTTCGTTAACAAGTTAACAAAACTA-3'
CG11322 gRNA2 5'- CTTCGCGACAGCAGTCGTAGTTCCA -3'
Sequencing primers for CG14814/GCNA
14814Arm1 Fwd Check caccGCCACCACAGAGAGTTCCAC
14814Arm2 rvs Check GTTGACGCTCTCCCTGTAGC
14814HA1 F Str2 caccCGACCCGAGCAAAGTAAAA
14814HA2 R Str2 GTAATGAGTCCAAGCATCGC
14814_orf_f1 CACTCGATTGGATAGCAGCA
14814_orf_r1 GCATCATCCACAGACAGCAT
14814_orf_f2 GCGCAAGTGGGTGATTCTTA
14814_orf_r2 ACGGTGTTTCCTTGCTTGTC

bedlam seq R3 TCCCCGAGAACACTTTCATC
bedlam seq F3 GAACAACGATACGCAGGTGA
FwdSeqpAFHW GGATACTCCTCCCGACACAAAG
Rev Seq pAFHW GGAAAGTCCTTGGGGTCTTC
SeqHAtagTransgeneFwd GCACGTTTGCTTGTTGAGAG
Sequencing primers for mh-GCNA
seqmh1-F TAGCCCTTGACTTGGTCTCC
seqmh2-R TCGTATCGCCTTTCATCTCA
seqmh3-R GCTAAATGCGGAGTCAGACC
Primers for generating Drosophila transgenes
14814_atgfwd caccATGGCGGATCATAAGTATAGGCTCTTCAATGCGG
14814_rev_clone
CTAGTTGGACGACTCGTCC
14814_rev_clone_NOSTOP
GTTGGACGACTCGTCCAGTGTC
for nls overlap
GGCAAATACGGAGGACACAG
geneblockcg14814nls5prime
caccATGGCGGATCATAAGTATAGGCTCTTCAATGCGGTCGACCCGAGCAAAGTAAAA GTTCCCTTCAATCAAAAGTTCGCCAATTTGACGCTATCCTCCCACAAAAAACGACTCC AGGTGTCCCATGCGCCGAAGGATCATCCAGAAAAGAGGAACGACCAGAAAACAAGG AAACTGCCAGCAGCTCCCATGCGCGCCAATGTGGGAGCACCCGCTCCGTCCTGCG GGGCAAATACGGAGGACACAGAA
SDM_AA_Fwd
CGTTGCACCTTGATAGCCGCACTCTGCCATGCTGC
SDM_AA_Rvs
GCAGCATGGCAGAGTGCGGCTATCAAGGTGCAACG
Triple tag endogenouse Tg for GCNA locus insert

GblockTripleTAG: ccGGTGGATCTGGAGGTTCCGGCGGCTCAGGGGGTAGTGTCAGCAAAGGAGAGGAG TTGATAAAGGAGAACATGCGTTCGAAACTGTATCTGGAGGGCAGCGTAAATGGACAC CAGTTCAAGTGCACGCATGAAGGAGAGGGCAAACCCTATGAAGGCAAACAAACGAA TCGGATTAAAGTAGTTGAAGGAGGTCCTCTCCCCTTCGCGTTCGACATCCTCGCCAC GCACTTCATGTACGGCTCCAAGGTATTCATTAAGTATCCAGCGGACCTCCCAGATTA CTTTAAGCAAAGTTTCCCAGAAGGTTTCACTTGGGAGCGAGTCATGGTCTTTGAAGA TGGAGGAGTTCTGACGGCTACACAGGACACTTCGTTGCAGGACGGCGAACTGATCT ACAACGTAAAGGTTCGGGGCGTGAACTTTCCAGCGAACGGACCCGTTATGCAAAAG AAGACGTTGGGATGGGAGCCTAGTACCGAAACTATGTATCCCGCCGATGGAGGCCT GGAAGGTAGGTGCGATAAAGCGCTCAAACTGGTCGGAGGTGGACACCTCCATGTAA ATTTCAAAACAACTTATAAGAGCAAAAAACCGGTGAAGATGCCGGGAGTGCACTACG TGGATCGGAGGTTGGAGCGAATAAAGGAGGCAGATAACGAGACGTATGTAGAACAG TACGAACACGCCGTCGCGCGATATAGCAACCTGGGCGGCGGCATGGACGAACTCTA CAAGGAGAGCAGCGGCAGCTACCCATACGATGTTCCAGATTACGCTGGATATCCATA TGATGTTCCAGATTATGCTGAGAGCAGCGGCAGCGACTACAAAGACCATGACGGTG ATTATAAAGATCATGACATCGATTACAAGGATGACGATGACAAGtga
TripleTagG-s1
CTTCGGACGAGTCGTCCAACTAGC
TripleTagG-as1
AAACGCTAGTTGGACGACTCGTCC
Seq-HA1embTT-F
CCATCACCCTCTTCCTGAAC
Seq-HA2embTT-R
AGCATCGCCTTTACCAACAC

APPENDIX B
Key Resource Table

REAGENT or RESOURCE	SOURCE	IDENTIFIER
Antibodies		
Mouse anti gamma-H2AV	DSHB	Cat#unc93.5.3.1
Rabbit anti-gamma-H2Av	(Mehrotra and McKim, 2006)	N/A
Rabbit anti-C(3)G	(Hong et al., 2003)	N/A
Rabbit anti-RPA	(Marton et al., 1994)	N/A
Rabbit anti-Top2	(Sander and Hsieh, 1983) (Gemkow et al., 2001)	N/A
Mouse anti-Hts	DSHB	Cat#1B1; RRID:AB_528070
Rat anti-Vasa	DSHB	Cat#vasa; RRID:AB_760351
Rabbit anti-GFP	Invitrogen	Cat#A-11122; RRID:AB_221569
Rat anti-HA	Roche	Cat#3F10; RRID:AB_2314622
Mouse anti-actin	DSHB	Cat#JLA20; RRID:AB_528068
Mouse anti-dsDNA	Abcam	Cat#Ab27156; RRID:AB_470907
Mouse anti-Lamin Dm0	DSHB	Cat#ADL84.12; RRID:AB_528338
Rat anti- tubulin [YL1/2]	Abcam	Cat#Ab6160; RRID:AB_305328
Rabbit Anti-Aubergine	(Nishida et al., 2007)	N/A
Rabbit anti-Rad-51	Sarit Smolikove	N/A
Mouse anti-FLAG M2	Sigma	Cat#F1807
Mouse anti-HA	Santa Cruz	Cat#F-7
OLLAS-tag Antibody, pAb, Rabbit	Genescript	Cat#9076
Guinea pig anti-XND-1	Yanowitz lab	N/A
Rabbit anti-gamma-H2Av	Amatruda lab	N/A
Goat Anti-Rabbit IgG (H+L)-HRP Conjugate	Bio-Rad	Cat#721019
Biological Samples		
DE Gold	Agilent	Cat#230132
Chemicals, Peptides, and Recombinant Proteins		
Hydroxyurea	Sigma- Aldrich	Cat#H8627; CAS:127-07-1
Pierce™ Trypsin Protease, MS Grade	Thermo Fisher Scientific	Cat#90057
4′,6-Diamidino-2-phenylindole dihydrochloride (DAPI)	Sigma-Aldrich	Cat#CD9542

Protease inhibitor	Roche	Cat#11836170001
Ni-NTA Superflow	Qiagen	Cat#30410
Centrifugal filter	Millipore	Cat#UFC910024
Q Sepharose	Sigma	Cat#Q1126
Trizol Reagent	Thermo Fisher Scientific	Cat#15596026
DNAse	Sigma	Cat#AMPD1
Paraformadehyde Aqueous Solution - 16% - 100mL	Electron Microscopy Sciences	Cat#27423
ProLong Gold Antifade Mountant with DAPI	Invitrogen	Cat#P36935
T4 DNA Polymerase	New England Biolabs	Cat#M0203S
Cas9 protein	PNA Bio	Cat#CP01-50
pCR4-TOPO TA cloning kit	Thermo-Fisher	Cat#K457502
Pronase	Sigma-Aldrich	Cat#11459643001
3,3′-Diaminobenzidine tetrahydrochloride	Sigma-Aldrich	Cat#D5905
Critical Commercial Assays		
Qiagen miRNeasy Mini kit	Qiagen	Cat#217004
DNAzol Reagent	Invitrogen	Cat#10503027
pENTR/D-TOPO Cloning Kit	Invitrogen	Cat#K240020
Gateway LR clonase	Invitrogen	Cat#11791019
Qiagen Plasmid Midi Kit	Qiagen	Cat#12143
QIAprep Spin Miniprep kit	Qiagen	Cat#27106
Effectene Transfection Reagent	Qiagen	Cat#301425
Quant-iT PicoGreen dsDNA Assay Kit	Invitrogen	Cat#P7589
ProteoSilver Silver Stain Kit	Sigma- Aldrich	Cat#PROTSIL1-1KT
Protoscript m-MuLV First Strand cDNA Synthesis kit	New England Biolabs	Cat#E6300S
SensiMix SYBR Hi-ROX kit	Bioline	Cat#QT-605
SMARTer® PCR cDNA Synthesis Kit	Takara/Clonetech	Cat#63925
Deposited Data		
Drosophila RNA-Seq	This paper	GEO: GSE127220
Experimental Models: Cell Lines		
S2R+ cells	Drosophila Genomics Resource Center	Cat#150; RRID: CVCL_Z831
Experimental Models: Organisms/Strains		
D. melanogaster: Df(1)BSC719	Bloomington Drosophila Stock Center	BDSC: 26571
D. melanogaster: Histone2Av.mRFP	Bloomington Drosophila Stock Center	BDSC: 23651
D. melanogaster: mh^{1} allele	Bloomington Drosophila Stock Center	BDSC: 7630
D. melanogaster: nos Gal4	(Inaba et al., 2015)	N/A
D. melanogaster: mei-$w68^{0949}$	(McKim and Hayashi-Hagihara, 1998)	N/A
D. melanogaster: mei-$P22^{1}$	(Liu et al., 2002)	N/A

D. melanogaster: p53-GFP reporter	(Wylie et al., 2014)	N/A
D. melanogaster: Gcna^{KO}	This paper	N/A
D. melanogaster: w; polo-GFP	D. Lerit	N/A
C. elegans: dog-1(gk10) I	Caenorhabditis Genetics Center	VC10
C. elegans: dog-1(gk10) I;*gcna-1(ea43)*	This paper	QP1910
C. elegans: dvc-1(ea65)/nT1[qIs51] V	This paper	QP1785
C. elegans: dvc-1(ok260) V	Caenorhabditis Genetics Center	RB1401
C. elegans: gcna-1(ea43) III/ hT2 [bli-4(e937) let-?(q782) qIs48] (I;III)	This paper	QP1664
C. elegans: gcna-1(ea43) III; *dvc-1(ea65)* V	This paper	QP1880
C. elegans: gcna-1(ea43) III;*spo-11(ok-79)* IV/ *nT1 [unc-?(n754) let-? qIs50]* (IV;V)	This paper	QP1892
C. elegans: gcna-1(ea43) III;*sws-1(ea12)* V	This paper	QP1788
C. elegans: gcna-1(ea43) III; *Top-2(av64)[TOP-2::3xFLAG]*	This paper	QP1894
C. elegans: gcna-1(ea67)[*ollas::gcna-1*]) III	This paper	QP1819
*C. elegans: gcna-1(*ea72 [*HA*::*gcna-1*]) III	This paper	QP1872
C. elegans: gcna-1(ea76) III/ hT2 [bli-4(e937) let-?(q782) qIs48] (I;III)	This paper	QP1891
C. elegans: gcna-1(ea80) exo-1(tm1842) III/ hT2 [bli-4(e937) let-?(q782) qIs48] (I;III)	This paper	QP1775
C. elegans: gcna-1(ea81) rfs-1(ok1372) III/ hT2 [bli-4(e937) let-?(q782) qIs48] (I;III)	This paper	QP1818
C. elegans: prg-1(n4357) I	Caenorhabditis Genetics Center	SX922
C. elegans: prg-1(n4357) I;*gcna-1(ea43)* III	This paper	QP1707
C. elegans: rfs-1(ok1372) III/ hT2 [bli-4(e937) let-?(q782) qIs48] (I;III)	This paper	QP1818
C. elegans: spo-11(ok79) IV/ *nT1 [unc-?(n754) let-? qIs50] (IV;V)*,	Yanowitz lab	QP600
C. elegans: sws-1(ea12) V	This paper	QP1208
C. elegans: Top-2(av64)[TOP-2::3xFLAG]	Aimee Jaramillo-Lambert	AG274
C. elegans: xpf-1(e1487) II	Caenorhabditis Genetics Center	CB1487
C. elegans: xpf-1(e1487) II; *gcna-1(ea43)* II	Caenorhabditis Genetics Center	QP1780
Oligonucleotides		
See Appendix A		
Recombinant DNA		
pU6-BbsI-chiRNA	M. Harrison, K. O'Connor-Giles, J. Wildonger	Addgene Plasmid #45946
pDsRed-attP or pHD-DsRed-attP	M. Harrison, K. O'Connor-Giles, J. Wildonger	Addgene Plasmid #51019

pPHW	Drosophila Genomics Resource Center	DGRC: 1101
pPWG	Drosophila Genomics Resource Center	DGRC: 1078
pAFHW	Drosophila Genomics Resource Center	DGRC: 1119
Cas9-SV40-H_6	Andy Golden, NIDDK	nm2973
Software and Algorithms		
FIJI (Fiji Is Just ImageJ)	NIH	https://imagej.net/Fiji/Downloads
Prism 7	GraphPad	N/A
Flycrispr design tool		http://flycrispr.molbio.wisc.edu/tools
Proteome Discoverer 2.1	Thermo Scientific	RRID:SRC:014477
Volocity 3D imaging software	Quorum Technologies (formally sold by PerkinElmer)	http://quorumtechnologies.com/volocity
C. elegans CRISPR design tool	Zhang lab, originally crispr.mit.edu	http://crispor.tefor.net/
Other		
^{137}Cs source	Nordion International	Gammacell 1000 Elite

BIBLIOGRAPHY

Abdu, U., Gonzalez-Reyes, A., Ghabrial, A., and Schupbach, T. (2003). The Drosophila spn-D gene encodes a RAD51C-like protein that is required exclusively during meiosis. Genetics *165*, 197-204.

Banani, S.F., Lee, H.O., Hyman, A.A., and Rosen, M.K. (2017). Biomolecular condensates: organizers of cellular biochemistry. Nat Rev Mol Cell Biol *18*, 285-298.

Batool, A., Karimi, N., Wu, X.N., Chen, S.R., and Liu, Y.X. (2019). Testicular germ cell tumor: a comprehensive review. Cell Mol Life Sci *76*, 1713-1727.

Bermejo, R., Capra, T., Gonzalez-Huici, V., Fachinetti, D., Cocito, A., Natoli, G., Katou, Y., Mori, H., Kurokawa, K., Shirahige, K., *et al.* (2009). Genome-organizing factors Top2 and Hmo1 prevent chromosome fragility at sites of S phase transcription. Cell *138*, 870-884.

Bettencourt-Dias, M., Rodrigues-Martins, A., Carpenter, L., Riparbelli, M., Lehmann, L., Gatt, M.K., Carmo, N., Balloux, F., Callaini, G., and Glover, D.M. (2005). SAK/PLK4 is required for centriole duplication and flagella development. Curr Biol *15*, 2199-2207.

Bianconi, E., Piovesan, A., Facchin, F., Beraudi, A., Casadei, R., Frabetti, F., Vitale, L., Pelleri, M.C., Tassani, S., Piva, F., *et al.* (2013). An estimation of the number of cells in the human body. Ann Hum Biol *40*, 463-471.

Blake-Hedges, C., and Megraw, T.L. (2019). Coordination of Embryogenesis by the Centrosome in Drosophila melanogaster. Results Probl Cell Differ *67*, 277-321.

Boese, C.J., Nye, J., Buster, D.W., McLamarrah, T.A., Byrnes, A.E., Slep, K.C., Rusan, N.M., and Rogers, G.C. (2018). Asterless is a Polo-like kinase 4 substrate that both activates and inhibits kinase activity depending on its phosphorylation state. Mol Biol Cell *29*, 2874-2886.

Borgermann, N., Ackermann, L., Schwertman, P., Hendriks, I.A., Thijssen, K., Liu, J.C., Lans, H., Nielsen, M.L., and Mailand, N. (2019). SUMOylation promotes protective responses to DNA-protein crosslinks. Embo j *38*.

Callaini, G., and Riparbelli, M.G. (1996). Fertilization in Drosophila melanogaster: centrosome inheritance and organization of the first mitotic spindle. Dev Biol *176*, 199-208.

Carmell, M.A., Dokshin, G.A., Skaletsky, H., Hu, Y.C., van Wolfswinkel, J.C., Igarashi, K.J., Bellott, D.W., Nefedov, M., Reddien, P.W., Enders, G.C., *et al.* (2016). A widely employed germ cell marker is an ancient disordered protein with reproductive functions in diverse eukaryotes. Elife *5*.

Carmena, M., Riparbelli, M.G., Minestrini, G., Tavares, A.M., Adams, R., Callaini, G., and Glover, D.M. (1998). Drosophila polo kinase is required for cytokinesis. J Cell Biol *143*, 659-671.

Chvalova, K., Brabec, V., and Kasparkova, J. (2007). Mechanism of the formation of DNA-protein cross-links by antitumor cisplatin. Nucleic Acids Res *35*, 1812-1821.

Colaiacovo, M.P., Stanfield, G.M., Reddy, K.C., Reinke, V., Kim, S.K., and Villeneuve, A.M. (2002). A targeted RNAi screen for genes involved in chromosome morphogenesis and nuclear organization in the Caenorhabditis elegans germline. Genetics *162*, 113-128.

Conduit, P.T., Feng, Z., Richens, J.H., Baumbach, J., Wainman, A., Bakshi, S.D., Dobbelaere, J., Johnson, S., Lea, S.M., and Raff, J.W. (2014). The centrosome-specific phosphorylation of Cnn by Polo/Plk1 drives Cnn scaffold assembly and centrosome maturation. Dev Cell *28*, 659-669.
Cortez, D., Glick, G., and Elledge, S.J. (2004). Minichromosome maintenance proteins are direct targets of the ATM and ATR checkpoint kinases. Proc Natl Acad Sci U S A *101*, 10078-10083.
Couch, F.B., Bansbach, C.E., Driscoll, R., Luzwick, J.W., Glick, G.G., Betous, R., Carroll, C.M., Jung, S.Y., Qin, J., Cimprich, K.A., *et al.* (2013). ATR phosphorylates SMARCAL1 to prevent replication fork collapse. Genes Dev *27*, 1610-1623.
Crasta, K., Ganem, N.J., Dagher, R., Lantermann, A.B., Ivanova, E.V., Pan, Y., Nezi, L., Protopopov, A., Chowdhury, D., and Pellman, D. (2012). DNA breaks and chromosome pulverization from errors in mitosis. Nature *482*, 53-58.
Davis, E.J., Lachaud, C., Appleton, P., Macartney, T.J., Nathke, I., and Rouse, J. (2012). DVC1 (C1orf124) recruits the p97 protein segregase to sites of DNA damage. Nat Struct Mol Biol *19*, 1093-1100.
Delabaere, L., Orsi, G.A., Sapey-Triomphe, L., Horard, B., Couble, P., and Loppin, B. (2014). The Spartan ortholog maternal haploid is required for paternal chromosome integrity in the Drosophila zygote. Curr Biol *24*, 2281-2287.
Dernburg, A.F., McDonald, K., Moulder, G., Barstead, R., Dresser, M., and Villeneuve, A.M. (1998). Meiotic recombination in C. elegans initiates by a conserved mechanism and is dispensable for homologous chromosome synapsis. Cell *94*, 387-398.
do Carmo Avides, M., Tavares, A., and Glover, D.M. (2001). Polo kinase and Asp are needed to promote the mitotic organizing activity of centrosomes. Nat Cell Biol *3*, 421-424.
Dobin, A., Davis, C.A., Schlesinger, F., Drenkow, J., Zaleski, C., Jha, S., Batut, P., Chaisson, M., and Gingeras, T.R. (2013). STAR: ultrafast universal RNA-seq aligner. Bioinformatics *29*, 15-21.
Donaldson, M.M., Tavares, A.A., Ohkura, H., Deak, P., and Glover, D.M. (2001). Metaphase arrest with centromere separation in polo mutants of Drosophila. J Cell Biol *153*, 663-676.
Eisman, R.C., Phelps, M.A., and Kaufman, T. (2015). An Amino-Terminal Polo Kinase Interaction Motif Acts in the Regulation of Centrosome Formation and Reveals a Novel Function for centrosomin (cnn) in Drosophila. Genetics *201*, 685-706.
Endow, S.A., and Komma, D.J. (1996). Centrosome and spindle function of the Drosophila Ncd microtubule motor visualized in live embryos using Ncd-GFP fusion proteins. Journal of Cell Science *109*, 2429-2442.
Ferree, P.M., and Barbash, D.A. (2009). Species-specific heterochromatin prevents mitotic chromosome segregation to cause hybrid lethality in Drosophila. PLoS Biol *7*, e1000234.
Gemkow, M.J., Dichter, J., and Arndt-Jovin, D.J. (2001). Developmental regulation of DNA-topoisomerases during Drosophila embryogenesis. Exp Cell Res *262*, 114-121.

Ghabrial, A., Ray, R.P., and Schupbach, T. (1998). okra and spindle-B encode components of the RAD52 DNA repair pathway and affect meiosis and patterning in Drosophila oogenesis. Genes Dev *12*, 2711-2723.
Goshima, G., Mayer, M., Zhang, N., Stuurman, N., and Vale, R.D. (2008). Augmin: a protein complex required for centrosome-independent microtubule generation within the spindle. J Cell Biol *181*, 421-429.
Gregan, J., Polakova, S., Zhang, L., Tolic-Norrelykke, I.M., and Cimini, D. (2011). Merotelic kinetochore attachment: causes and effects. Trends Cell Biol *21*, 374-381.
Halazonetis, T.D., Gorgoulis, V.G., and Bartek, J. (2008). An oncogene-induced DNA damage model for cancer development. Science *319*, 1352-1355.
Halder, S., Torrecilla, I., Burkhalter, M.D., Popovic, M., Fielden, J., Vaz, B., Oehler, J., Pilger, D., Lessel, D., Wiseman, K., *et al.* (2019). SPRTN protease and checkpoint kinase 1 cross-activation loop safeguards DNA replication. Nat Commun *10*, 3142.
Hatch, E.M., Fischer, A.H., Deerinck, T.J., and Hetzer, M.W. (2013). Catastrophic nuclear envelope collapse in cancer cell micronuclei. Cell *154*, 47-60.
Hatsumi, M., and Endow, S.A. (1992). The Drosophila ncd microtubule motor protein is spindle-associated in meiotic and mitotic cells. J Cell Sci *103 (Pt 4)*, 1013-1020.
Helmrich, A., Ballarino, M., and Tora, L. (2011). Collisions between replication and transcription complexes cause common fragile site instability at the longest human genes. Mol Cell *44*, 966-977.
Hillers, K.J., Jantsch, V., Martinez-Perez, E., and Yanowitz, J.L. (2017). Meiosis. WormBook *2017*, 1-43.
Hodgkin, J., Horvitz, H.R., and Brenner, S. (1979). Nondisjunction Mutants of the Nematode CAENORHABDITIS ELEGANS. Genetics *91*, 67-94.
Hong, A., Lee-Kong, S., Iida, T., Sugimura, I., and Lilly, M.A. (2003). The p27cip/kip ortholog dacapo maintains the Drosophila oocyte in prophase of meiosis I. Development (Cambridge, England) *130*, 1235-1242.
Inaba, M., Buszczak, M., and Yamashita, Y.M. (2015). Nanotubes mediate niche-stem-cell signalling in the Drosophila testis. Nature *523*, 329-332.
Jang, J.K., Sherizen, D.E., Bhagat, R., Manheim, E.A., and McKim, K.S. (2003). Relationship of DNA double-strand breaks to synapsis in Drosophila. J Cell Sci *116*, 3069-3077.
Janning, W. (1978). Gynandromorph fate maps in Drosophila. Results Probl Cell Differ *9*, 1-28.
Jin, Y., Tam, O.H., Paniagua, E., and Hammell, M. (2015). TEtranscripts: a package for including transposable elements in differential expression analysis of RNA-seq datasets. Bioinformatics *31*, 3593-3599.
Joyce, E.F., Pedersen, M., Tiong, S., White-Brown, S.K., Paul, A., Campbell, S.D., and McKim, K.S. (2011). Drosophila ATM and ATR have distinct activities in the regulation of meiotic DNA damage and repair. J Cell Biol *195*, 359-367.
Keeney, S., Giroux, C.N., and Kleckner, N. (1997). Meiosis-specific DNA double-strand breaks are catalyzed by Spo11, a member of a widely conserved protein family. Cell *88*, 375-384.

Kiianitsa, K., and Maizels, N. (2013). A rapid and sensitive assay for DNA-protein covalent complexes in living cells. Nucleic Acids Res *41*, e104.
Koundrioukoff, S., Carignon, S., Techer, H., Letessier, A., Brison, O., and Debatisse, M. (2013). Stepwise activation of the ATR signaling pathway upon increasing replication stress impacts fragile site integrity. PLoS Genet *9*, e1003643.
Krishnakumar, P., and Dosch, R. (2018). Germ Cell Specification: The Evolution of a Recipe to Make Germ Cells. In Germ Cell.
Kruisselbrink, E., Guryev, V., Brouwer, K., Pontier, D.B., Cuppen, E., and Tijsterman, M. (2008). Mutagenic capacity of endogenous G4 DNA underlies genome instability in FANCJ-defective C. elegans. Curr Biol *18*, 900-905.
Kurimoto, K., and Saitou, M. (2018). Epigenome regulation during germ cell specification and development from pluripotent stem cells. Curr Opin Genet Dev *52*, 57-64.
Larsen, N.B., Gao, A.O., Sparks, J.L., Gallina, I., Wu, R.A., Mann, M., Raschle, M., Walter, J.C., and Duxin, J.P. (2019). Replication-Coupled DNA-Protein Crosslink Repair by SPRTN and the Proteasome in Xenopus Egg Extracts. Mol Cell *73*, 574-588.e577.
Liu, H., Jang, J.K., Kato, N., and McKim, K.S. (2002). mei-P22 encodes a chromosome-associated protein required for the initiation of meiotic recombination in Drosophila melanogaster. Genetics *162*, 245-258.
Llamazares, S., Moreira, A., Tavares, A., Girdham, C., Spruce, B.A., Gonzalez, C., Karess, R.E., Glover, D.M., and Sunkel, C.E. (1991). polo encodes a protein kinase homolog required for mitosis in Drosophila. Genes Dev *5*, 2153-2165.
Lopes, M., Cotta-Ramusino, C., Pellicioli, A., Liberi, G., Plevani, P., Muzi-Falconi, M., Newlon, C.S., and Foiani, M. (2001). The DNA replication checkpoint response stabilizes stalled replication forks. Nature *412*, 557-561.
Lopez-Mosqueda, J., Maddi, K., Prgomet, S., Kalayil, S., Marinovic-Terzic, I., Terzic, J., and Dikic, I. (2016). SPRTN is a mammalian DNA-binding metalloprotease that resolves DNA-protein crosslinks. Elife *5*.
Love, M.I., Huber, W., and Anders, S. (2014). Moderated estimation of fold change and dispersion for RNA-seq data with DESeq2. Genome Biol *15*, 550.
Lu, W.J., Chapo, J., Roig, I., and Abrams, J.M. (2010). Meiotic recombination provokes functional activation of the p53 regulatory network. Science *328*, 1278-1281.
Ly, P., Teitz, L.S., Kim, D.H., Shoshani, O., Skaletsky, H., Fachinetti, D., Page, D.C., and Cleveland, D.W. (2017). Selective Y centromere inactivation triggers chromosome shattering in micronuclei and repair by non-homologous end joining. Nat Cell Biol *19*, 68-75.
Magdalou, I., Lopez, B.S., Pasero, P., and Lambert, S.A. (2014). The causes of replication stress and their consequences on genome stability and cell fate. Semin Cell Dev Biol *30*, 154-164.
Mani, S.R., Megosh, H., and Lin, H. (2014). PIWI proteins are essential for early Drosophila embryogenesis. Dev Biol *385*, 340-349.
Mankouri, H.W., Huttner, D., and Hickson, I.D. (2013). How unfinished business from S-phase affects mitosis and beyond. Embo j *32*, 2661-2671.

Mantiero, D., Mackenzie, A., Donaldson, A., and Zegerman, P. (2011). Limiting replication initiation factors execute the temporal programme of origin firing in budding yeast. Embo j *30*, 4805-4814.
Marton, R.F., Thommes, P., and Cotterill, S. (1994). Purification and characterisation of dRP-A: a single-stranded DNA binding protein from Drosophila melanogaster. FEBS Lett *342*, 139-144.
McKim, K.S., and Hayashi-Hagihara, A. (1998). mei-W68 in Drosophila melanogaster encodes a Spo11 homolog: evidence that the mechanism for initiating meiotic recombination is conserved. Genes Dev *12*, 2932-2942.
Mehrotra, S., and McKim, K.S. (2006). Temporal analysis of meiotic DNA double-strand break formation and repair in Drosophila females. PLoS Genet *2*, e200.
Milholland, B., Dong, X., Zhang, L., Hao, X., Suh, Y., and Vijg, J. (2017). Differences between germline and somatic mutation rates in humans and mice. Nat Commun *8*, 15183.
Morocz, M., Zsigmond, E., Toth, R., Enyedi, M.Z., Pinter, L., and Haracska, L. (2017). DNA-dependent protease activity of human Spartan facilitates replication of DNA-protein crosslink-containing DNA. Nucleic Acids Res *45*, 3172-3188.
Mosbech, A., Gibbs-Seymour, I., Kagias, K., Thorslund, T., Beli, P., Povlsen, L., Nielsen, S.V., Smedegaard, S., Sedgwick, G., Lukas, C., *et al.* (2012). DVC1 (C1orf124) is a DNA damage-targeting p97 adaptor that promotes ubiquitin-dependent responses to replication blocks. Nat Struct Mol Biol *19*, 1084-1092.
Murai, J., Huang, S.Y., Das, B.B., Renaud, A., Zhang, Y., Doroshow, J.H., Ji, J., Takeda, S., and Pommier, Y. (2012). Trapping of PARP1 and PARP2 by Clinical PARP Inhibitors. Cancer Res *72*, 5588-5599.
Neale, M.J., Pan, J., and Keeney, S. (2005). Endonucleolytic processing of covalent protein-linked DNA double-strand breaks. Nature *436*, 1053-1057.
Nelson, C.R., and Szauter, P. (1992). Timing of mitotic chromosome loss caused by the ncd mutation of Drosophila melanogaster. Cell Motil Cytoskeleton *23*, 34-44.
Nishida, K.M., Saito, K., Mori, T., Kawamura, Y., Nagami-Okada, T., Inagaki, S., Siomi, H., and Siomi, M.C. (2007). Gene silencing mechanisms mediated by Aubergine piRNA complexes in Drosophila male gonad. Rna *13*, 1911-1922.
Nott, T.J., Petsalaki, E., Farber, P., Jervis, D., Fussner, E., Plochowietz, A., Craggs, T.D., Bazett-Jones, D.P., Pawson, T., Forman-Kay, J.D., *et al.* (2015). Phase transition of a disordered nuage protein generates environmentally responsive membraneless organelles. Mol Cell *57*, 936-947.
Page, S.L., and Hawley, R.S. (2001). c(3)G encodes a Drosophila synaptonemal complex protein. Genes Dev *15*, 3130-3143.
Petry, S. (2016). Mechanisms of Mitotic Spindle Assembly. Annu Rev Biochem *85*, 659-683.
Pommier, Y., Huang, S.Y., Gao, R., Das, B.B., Murai, J., and Marchand, C. (2014). Tyrosyl-DNA-phosphodiesterases (TDP1 and TDP2). DNA Repair (Amst) *19*, 114-129.
Riparbelli, M.G., Callaini, G., and Glover, D.M. (2000). Failure of pronuclear migration and repeated divisions of polar body nuclei associated with MTOC defects in polo eggs of Drosophila. J Cell Sci *113 (Pt 18)*, 3341-3350.

Sale, J.E., Lehmann, A.R., and Woodgate, R. (2012). Y-family DNA polymerases and their role in tolerance of cellular DNA damage. Nat Rev Mol Cell Biol *13*, 141-152.
Sander, M., and Hsieh, T. (1983). Double strand DNA cleavage by type II DNA topoisomerase from Drosophila melanogaster. J Biol Chem *258*, 8421-8428.
Sauer, G., Korner, R., Hanisch, A., Ries, A., Nigg, E.A., and Sillje, H.H. (2005). Proteome analysis of the human mitotic spindle. Mol Cell Proteomics *4*, 35-43.
Savoian, M.S., and Glover, D.M. (2014). Differing requirements for Augmin in male meiotic and mitotic spindle formation in Drosophila. Open Biol *4*, 140047.
Schatten, H., and Sun, Q.Y. (2009). The role of centrosomes in mammalian fertilization and its significance for ICSI. Mol Hum Reprod *15*, 531-538.
Seydoux, G. (2018). The P Granules of C. elegans: A Genetic Model for the Study of RNA-Protein Condensates. J Mol Biol.
Sharp, D.J., McDonald, K.L., Brown, H.M., Matthies, H.J., Walczak, C., Vale, R.D., Mitchison, T.J., and Scholey, J.M. (1999). The bipolar kinesin, KLP61F, cross-links microtubules within interpolar microtubule bundles of Drosophila embryonic mitotic spindles. J Cell Biol *144*, 125-138.
Silk, A.D., Zasadil, L.M., Holland, A.J., Vitre, B., Cleveland, D.W., and Weaver, B.A. (2013). Chromosome missegregation rate predicts whether aneuploidy will promote or suppress tumors. Proc Natl Acad Sci U S A *110*, E4134-4141.
Sköld, H.N., Komma, D.J., and Endow, S.A. (2005). Assembly pathway of the anastral *Drosophila* oocyte meiosis I spindle. Journal of Cell Science *118*, 1745-1755.
Smith, J., Calidas, D., Schmidt, H., Lu, T., Rasoloson, D., and Seydoux, G. (2016). Spatial patterning of P granules by RNA-induced phase separation of the intrinsically-disordered protein MEG-3. Elife *5*.
Soper, S.F., van der Heijden, G.W., Hardiman, T.C., Goodheart, M., Martin, S.L., de Boer, P., and Bortvin, A. (2008). Mouse maelstrom, a component of nuage, is essential for spermatogenesis and transposon repression in meiosis. Dev Cell *15*, 285-297.
Staeva-Vieira, E., Yoo, S., and Lehmann, R. (2003). An essential role of DmRad51/SpnA in DNA repair and meiotic checkpoint control. Embo j *22*, 5863-5874.
Stephens, P.J., Greenman, C.D., Fu, B., Yang, F., Bignell, G.R., Mudie, L.J., Pleasance, E.D., Lau, K.W., Beare, D., Stebbings, L.A., *et al.* (2011). Massive genomic rearrangement acquired in a single catastrophic event during cancer development. Cell *144*, 27-40.
Stingele, J., Bellelli, R., Alte, F., Hewitt, G., Sarek, G., Maslen, S.L., Tsutakawa, S.E., Borg, A., Kjaer, S., Tainer, J.A., *et al.* (2016). Mechanism and Regulation of DNA-Protein Crosslink Repair by the DNA-Dependent Metalloprotease SPRTN. Mol Cell *64*, 688-703.
Stingele, J., Bellelli, R., and Boulton, S.J. (2017). Mechanisms of DNA-protein crosslink repair. Nat Rev Mol Cell Biol *18*, 563-573.
Sun, Q.Y., and Schatten, H. (2007). Centrosome inheritance after fertilization and nuclear transfer in mammals. Adv Exp Med Biol *591*, 58-71.
Sung, P. (1994). Catalysis of ATP-dependent homologous DNA pairing and strand exchange by yeast RAD51 protein. Science *265*, 1241-1243.

Szalontai, T., Gaspar, I., Belecz, I., Kerekes, I., Erdelyi, M., Boros, I., and Szabad, J. (2009). HorkaD, a chromosome instability-causing mutation in Drosophila, is a dominant-negative allele of Lodestar. Genetics *181*, 367-377.
Tang, W.W., Kobayashi, T., Irie, N., Dietmann, S., and Surani, M.A. (2016). Specification and epigenetic programming of the human germ line. Nat Rev Genet *17*, 585-600.
Tang, X., Cao, J., Zhang, L., Huang, Y., Zhang, Q., and Rong, Y.S. (2017). Maternal Haploid, a Metalloprotease Enriched at the Largest Satellite Repeat and Essential for Genome Integrity in Drosophila Embryos. Genetics *206*, 1829-1839.
Tastan, O.Y., Maines, J.Z., Li, Y., McKearin, D.M., and Buszczak, M. (2010). Drosophila ataxin 2-binding protein 1 marks an intermediate step in the molecular differentiation of female germline cysts. Development *137*, 3167-3176.
Tercero, J.A., and Diffley, J.F. (2001). Regulation of DNA replication fork progression through damaged DNA by the Mec1/Rad53 checkpoint. Nature *412*, 553-557.
Toledo, L.I., Altmeyer, M., Rask, M.B., Lukas, C., Larsen, D.H., Povlsen, L.K., Bekker-Jensen, S., Mailand, N., Bartek, J., and Lukas, J. (2013). ATR prohibits replication catastrophe by preventing global exhaustion of RPA. Cell *155*, 1088-1103.
Tuduri, S., Crabbe, L., Conti, C., Tourriere, H., Holtgreve-Grez, H., Jauch, A., Pantesco, V., De Vos, J., Thomas, A., Theillet, C., *et al.* (2009). Topoisomerase I suppresses genomic instability by preventing interference between replication and transcription. Nat Cell Biol *11*, 1315-1324.
Uebel, C.J., Anderson, D.C., Mandarino, L.M., Manage, K.I., Aynaszyan, S., and Phillips, C.M. (2018). Distinct regions of the intrinsically disordered protein MUT-16 mediate assembly of a small RNA amplification complex and promote phase separation of Mutator foci. PLoS Genet *14*, e1007542.
Uehara, R., Nozawa, R.S., Tomioka, A., Petry, S., Vale, R.D., Obuse, C., and Goshima, G. (2009). The augmin complex plays a critical role in spindle microtubule generation for mitotic progression and cytokinesis in human cells. Proc Natl Acad Sci U S A *106*, 6998-7003.
Vaz, B., Popovic, M., Newman, J.A., Fielden, J., Aitkenhead, H., Halder, S., Singh, A.N., Vendrell, I., Fischer, R., Torrecilla, I., *et al.* (2016). Metalloprotease SPRTN/DVC1 Orchestrates Replication-Coupled DNA-Protein Crosslink Repair. Mol Cell *64*, 704-719.
Vaz, B., Popovic, M., and Ramadan, K. (2017). DNA-Protein Crosslink Proteolysis Repair. Trends Biochem Sci *42*, 483-495.
Walport, L.J., Hopkinson, R.J., and Schofield, C.J. (2012). Mechanisms of human histone and nucleic acid demethylases. Curr Opin Chem Biol *16*, 525-534.
Weinstein, J.N., Collisson, E.A., Mills, G.B., Shaw, K.R., Ozenberger, B.A., Ellrott, K., Shmulevich, I., Sander, C., and Stuart, J.M. (2013). The Cancer Genome Atlas Pan-Cancer analysis project. Nat Genet *45*, 1113-1120.
Wilhelm, T., Magdalou, I., Barascu, A., Techer, H., Debatisse, M., and Lopez, B.S. (2014). Spontaneous slow replication fork progression elicits mitosis alterations in homologous recombination-deficient mammalian cells. Proc Natl Acad Sci U S A *111*, 763-768.

Williams, B.R., Prabhu, V.R., Hunter, K.E., Glazier, C.M., Whittaker, C.A., Housman, D.E., and Amon, A. (2008). Aneuploidy affects proliferation and spontaneous immortalization in mammalian cells. Science *322*, 703-709.
Wylie, A., Lu, W.J., D'Brot, A., Buszczak, M., and Abrams, J.M. (2014). p53 activity is selectively licensed in the Drosophila stem cell compartment. Elife *3*, e01530.
Youds, J.L., Barber, L.J., Ward, J.D., Collis, S.J., O'Neil, N.J., Boulton, S.J., and Rose, A.M. (2008). DOG-1 is the Caenorhabditis elegans BRIP1/FANCJ homologue and functions in interstrand cross-link repair. Mol Cell Biol *28*, 1470-1479.
Zegerman, P., and Diffley, J.F. (2010). Checkpoint-dependent inhibition of DNA replication initiation by Sld3 and Dbf4 phosphorylation. Nature *467*, 474-478.
Zhang, B.N., Bueno Venegas, A., Hickson, I.D., and Chu, W.K. (2018). DNA replication stress and its impact on chromosome segregation and tumorigenesis. Semin Cancer Biol.
Zhang, J., and Megraw, T.L. (2007). Proper recruitment of gamma-tubulin and D-TACC/Msps to embryonic Drosophila centrosomes requires Centrosomin Motif 1. Mol Biol Cell *18*, 4037-4049.
Zhao, D., McBride, D., Nandi, S., McQueen, H.A., McGrew, M.J., Hocking, P.M., Lewis, P.D., Sang, H.M., and Clinton, M. (2010). Somatic sex identity is cell autonomous in the chicken. Nature *464*, 237-242.